

Title

Carlos G. Oliver

Master of Science

Department of Biology

McGill University

Montreal, Quebec

August 5, 2016

A thesis submitted to McGill University in partial fulfillment of the requirements of
the degree of Master of Science

©Carlos G. Oliver, 2016

DEDICATION

This document is dedicated to the graduate students of the McGill University.

ACKNOWLEDGEMENTS

Acknowledgments, if included, must be written in complete sentences. Do not use direct address. For example, instead of Thanks, Mom and Dad!, you should say I thank my parents.

CONTRIBUTION OF AUTHORS

All data collection and results obtained during my M.Sc. are presented here as a standard format thesis. This work includes results and figures obtained by collaborators in the Department of Chemistry Dr. Anthony Mittermaier and Jason Harris who conducted NMR experiments and generated all NMR based figures. All computer simulation work and MD figures were done by myself. All text and literature review in this thesis was done by myself with feedback from my supervisor Jackie Vogel and collaborator Anthony Mittermaier.

ABSTRACT

Abstract in English and French are required. The text of the abstract in English begins here.

ABRÉGÉ

The text of the abstract in French begins here.

TABLE OF CONTENTS

DEDICATION	ii
ACKNOWLEDGEMENTS	iii
CONTRIBUTION OF AUTHORS	iv
ABSTRACT	v
ABRÉGÉ	vi
LIST OF FIGURES	ix
KEY TO ABBREVIATIONS	x
1 Introduction	1
1.1 Disorder in proteins	3
1.2 Physical mechanisms of IDP function in cellular machines	6
1.3 IDP function in the mitotic spindle	10
1.3.1 Microtubules	10
1.3.2 γ -Tubulin & the γ -CT	11
1.4 Experimental question	12
1.5 Approach	13
2 Theory & Methods	14
2.1 Molecular Dynamics Simulations	15
2.1.1 Computing trajectories of atoms	15
2.1.2 Force Field	16
2.1.3 Preparing the system	18
2.2 Trajectory Analysis	19
2.2.1 Root Mean Square Deviation	19
2.2.2 Radius of gyration	20
2.2.3 Diffusion coefficient and Hydrodynamic Radius	20

2.2.4	Covariance Analysis	21
3	Conformational analysis of the γ -Tubulincarboxyl terminus	24
3.1	NMR	25
3.2	Setting up the MD runs	26
3.3	Conformational sampling of γ -CT isoforms	28
3.3.1	Collective motions correspond to transitions between extended and collapsed conformations	37
3.3.2	Whole protein simulations and conserved properties of γ -CT	42
3.4	Discussion	43
4	Conclusions	48
4.0.1	Summary of Findings	48
4.0.2	Future Aims	48
5	Appendix	50
	References	55

LIST OF FIGURES

<u>Figure</u>	<u>page</u>
1–1 γ -Tubulin 3D Structure	4
3–1 γ -CT Secondary Structure Assignments	29
3–2 RMSD	31
3–3 γ -CT predicted conformational ensemble	32
3–4 Distribution of diffusion coefficients	34
3–5 Time-series plot of D_t over 2 μ s simulation.	35
3–6 Distribution of diffusion coefficients	38
3–7 eigenvalues	39
3–8 Principal Component Analysis	41
3–9 porcupine plot	41
3–10 γ -Tubulinfull protein simulation	43
3–11 Multiple Sequence Alinment of γ -CT across eukaryotes	44
3–12 IDP Conformational Landscapes	46
3–13 γ -TuRC	47
5–1 NMR Secondary Structure Assignments	51
5–2 NMR Chemical Shifts	51
5–3 NMR Diffusion Measurements	52
5–4 NMR Dispersion Measurements	52
5–4 Tubulin CT Multiple Sequence Alignments	54

KEY TO ABBREVIATIONS

D_t : Translational Diffusion Coefficient

R_g : Radius of Gyration

γ -CT: γ -Tubulin C-Terminus

γ -TuRC: γ -Tubulin Ring Complex

μ s: Microsecond

CBP: CREB Binding Protein

CREB: Cyclic AMP Response Element Binding Protein

DNA: Deoxyribonucleic Acid

GRIPS: γ -Tubulin Ring Proteins

GROMACS: GROnigen Machine for Chemical Simulatoins

IDP: Intrinsically Disordered Protein

IDR: Intrinsically Disordered Region

KID: Kinase Inducible Domain

MD: Molecular Dynamics

NMR: Nuclear Magnetic Resonance

NPT: Isothermal-isobaric Ensemble

ns: Nanosecond

NVE: Microcanonical Ensemble

NVT: Canonical Ensemble

OPLS-AA: Optimized Potential for Liquid Simulations - All Atom

PTM: Post-Translational Modification

RMSD: Root Mean Square Displacement

SPCE: Extended Single Point Charge

VMD: Visual Molecular Dynamics

WT: Wild-Type

YD: Y445D mutant

CHAPTER 1

Introduction

Everything existing in the universe
is the fruit of chance and necessity.

Democritus

Molecular machines are assemblies of proteins that interact in a coordinated manner to solve a biological problem. These biological problems, such as coordinating chromosome separation during cell division, cell cycle timing, protein synthesis, etc. cover many processes essential to life. Given the necessity for survival in the face of ever changing environments, evolution has produced a large diversity of molecular mechanisms for solving these problems in a flexible yet robust manner. A machine that only functions properly under unchanging conditions and inputs is not likely to survive in a biological context. Therefore, at the core of each of those processes are highly complex networks of protein interactions that are able to assemble, communicate, coordinate, self-regulate and self-correct in order to accomplish the necessary task reliably. For example, the vital process of DNA replication is executed by a large multitude of proteins that each contribute to the process of copying the genome. The replication machinery must read environmental cues for initiating replication at the correct time, meanwhile complex combinatoric signaling networks ensure that DNA replication unfolds in a processive manner, enzymatic components perform physical work by unwinding the DNA strand for copying, and others communicate with the

DNA repair machinery to correct copying errors and avoid harmful mutations. It is clear that solving this biological problem requires the ability of participating proteins to interact with many different partners and mediate many different processes.

The way proteins are able to control interactions and drive function is through the conformational arrangement of their backbones which is encoded in each protein's amino acid sequence. Specific spatial arrangements of peptide chains, also known as protein structure, allows for specific interactions between proteins to assemble molecular machines, recruit necessary factors and mediate necessary chemical reactions. See **Fig. ??** for a visualization of protein structure. Since the 1950s when the first X-ray crystallography protein structure was solved, we have learned a great deal about how 3D architecture and motions of the chains give rise to protein function. By capturing various conformations of folded protein domains, we have been able to infer that coordinated motions between structural conformations is the main element of control in protein function. For example, X-ray crystallography experiments have shown that the activity of Calmodulin, an important signalling protein is modulated by conformational changes of its α -helix domains brought about by binding of Ca^+ ions [20]. These conformational rearrangements initiate a clamping motion of the helical domains which allow Calmodulin to bind to its downstream targets. However, it is important to note that X-ray crystallography only offers static pictures of protein structure, and provides information mostly on the spatial arrangement of relatively large stable domains in proteins. It therefore became a long standing dogma that the stable 3D folds of a protein chain dictate a protein's function, also known as the "one structure - one function" paradigm. Yet, as we saw with DNA

replication, molecular processes are incredibly complex. A single protein is often required to fulfill many functions, interact with various different partners and be able to do so on very fast timescales. It is therefore unlikely that such large scale and consequently slow structural motions can account for all of the precise and rapid control we observe in biological systems. A static description of proteins is not sufficient to explain the degree of functional flexibility and control that we observe. This leaves us with several questions. If one structure means one function, how can the same protein fulfill multiple functions and engage in many different interactions? How can molecular machines offer such precise control of functionality while counting only on a static architectures? The broad aim of this thesis is therefore to improve our understanding of the physical mechanisms underlying the functional complexity of molecular machines.

1.1 Disorder in proteins

One potential source of functional plasticity can be found in regions of proteins that do not adopt stable architectures, also known as intrinsically disordered proteins (IDPs). While IDPs are highly flexible and largely unstructured, functional studies have shown that they are necessary for many cellular processes.¹ Instead of relying on a structure for function, IDP functionality lies the absence of structure. This flexibility offers the protein rapid access to a vast pool of conformations with which

¹ We will use the term IDP loosely to denote any unstructured protein element. Some works make the distinction between IDP and IDR where an IDR is an intrinsically disordered region and is not a full protein. There will be instances in the text where we will use IDR in this way.

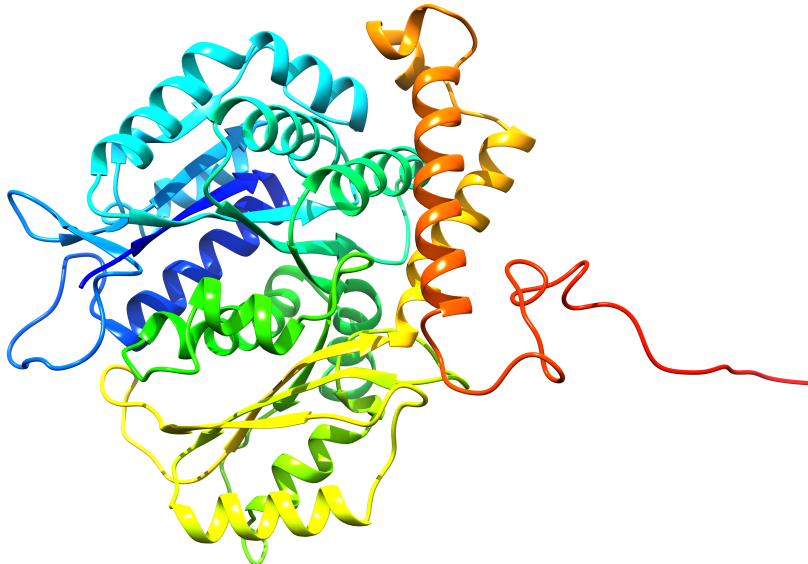


Figure 1–1: γ -Tubulin 3D Structure

Visual representation of the yeast γ -Tubulin protein based on the human γ -Tubulin structure derived from X-ray crystallography [1]. The protein is composed of a highly ordered globular domain stabilized by various α -helices and β -sheet domains and measures 2.20 nm in radius of gyration. In red, we see the disordered γ -CT region which was absent in the crystal structure and was modeled by RaptorX.

to fine-tune and diversify its function. Many examples have now been described where IDPs flexibility is used to dynamically regulate binding, mediate signaling, impose thresholds, and sense environmental queues.

For a long time, these types of protein element were overlooked in favour of studying stable folding patterns. IDRs were thought to act simply as flexible linkers between structural domains without any function of their own. This was also due in part to the fact that the main tool being used for structural biology, X-ray crystallography, fails to detect patterns in unfolded chains, making it difficult to study

The lack of structure in IDPs can be explained by their characteristic low sequence complexities, and an enrichment for polar and charged residues over

highly dynamic elements in protein such as IDPs. Techniques that do produce information on dynamics such as NMR only developed for proteins until much later. The first protein structure solved by X-ray crystallography was in 1958 and it was not until 1984 that the first protein structure was solved using NMR. Likewise, until recently, computational tools to study protein dynamics *ab initio*, such as Molecular Dynamics (MD) were greatly limited by shortcomings in processor power. However, with large advances in experimental and computational techniques in recent years, we have been able to study the dynamic properties of IDEs in great detail, and have found that they play key roles in the functioning of molecular machines.

Given the prevalence of disorder in proteins, it is not surprising that IDPs have been implicated in a multitude of cellular processes and disease states through NMR and mutational studies. These processes include signalling, cell cycle control, transcription, translation, ribosome assembly, chromatin organization, microtubule assembly/disassembly, etc [29]. Interestingly, it has been shown that viral proteins use IDPs in their proteins to hijack cellular proteins and use the flexibility of IDPs to mimic host proteins and recruit host cellular machinery in order to propagate.[4] This would suggest that viral proteins use IDPs to make efficient use of their smaller genomes and obtain a greater range of function from the limited number of proteins in their genomes. It is now clear that IDPs, through their lack of structure, are an important adaptive feature that drive the functional complexity and robustness we observe in molecular machines.

1.2 Physical mechanisms of IDP function in cellular machines

In this section we will give a brief account of some of the physical mechanisms of IDP function that have been described in the literature.

Phosphorylation

A key aspect of dynamic control is the ability to modulate function in a precise and reversible manner. The cell needs to be able to induce and inhibit interactions in a time and space dependent manner. To solve this problem, the cell harnesses the structural malleability of IDPs by coupling it with post translational modifications, most commonly, phosphorylation. Phosphorylation is the reversible covalent addition of a phosphate group, which carries a negative charge, to one a tyrosine or serine amino acid by a kinase enzyme. The reverse reaction is catalyzed by enzymes called proteases which remove the phosphate group. The addition of a phosphate group introduces the potential for hydrogen bonding with itself and with other targets, and alters the electrostatic environment of the IDP. This change can therefore bias the stochastic conformational sampling of the IDP in a particular direction, and because it is reversible, it acts as a means for driving structural switching which can then be used to modulate a large range of interactions. Not surprisingly, it has been seen in many studies that IDPs are prime targets for phosphorylation *in vivo*. The use of phosphorylation as an information carrier has been described in various cellular systems. For example, in cell cycle control, there is a strong need for a specific temporal sequence of interactions to be enforced. Therefore, the sequential phosphorylation of a single target can modify the affinity for the same

target to the next target in the pathway, ensuring that interactions take place in an ordered manner. Phosphorylation can also be used to enforce thresholds, where in order to avoid the negative impact of accidental interactions, certain interactions will be blocked until an IDP has achieved a certain number of phosphorylations. Having accumulated enough phosphorylations, a structural rearrangement favours the interaction.

word this better

Disorder-Order transitions

The best explored physical mechanism of IDP function is the fold-on binding paradigm [28]. In this case, IDPs in the free form are unstructured, and when they encounter their binding target, they undergo a folding transition (disorder to order) to form a stable complex. The lack of structure in the unbound state allows the IDP to recognize multiple targets, and it allows binding to be inducible instead of constitutive. A well studied example of this kind of mechanism is the binding of the transcriptional activator protein CREB and its co-activator CBP [9]. An IDR in CREB known as KID mediates binding to CBP where upon binding, the IDP folds into a pair of helices. However, this binding process is not favoured spontaneously

due to loss of entropy induced by folding.² However, when the KID is phosphorylated, the phosphoryl group interacts with CBP by forming hydrogen bonds which result in a negative enthalpic change that compensates for the loss of entropy and thus makes the folding reaction favourable. Because of the inducible nature of this interaction, CBP is able to also interact with other co-factors, which has been reported in the literature [22]. This is an example of how even though the association state of the IDP is ordered, it is the intrinsic disorder and entropy of the unbound state which acts as a tool for controlling the interaction.

² We consider the expression for Gibbs free energy, $\Delta G = \Delta H - T\Delta S$, where ΔH is the change in enthalpy, or heat energy available to the system, and ΔS is the entropy, or degree of disorder/conformational freedom available to the system. If we define our system as a protein chain, we see that a decrease in entropy which can be brought upon by the ordering of a structure will result in a positive ΔG thus making the reaction energetically unfavourable. This loss of entropy, or conformational freedom, can be overcome by a release of heat, or a sufficiently negative ΔH component which can tip the energetic balance toward $\Delta G < 0$. One might say that the decrease in entropy in the protein would be in violation of the second law of thermodynamics which states that all systems tend toward an increase in entropy. However, a reaction with a negative ΔH , in other words, a reaction releasing heat will cause an increase in entropy to its surrounding environment. In the case of protein, the process of folding will reduce the entropy of the protein, but if the folding has a negative ΔH it will release heat and thus increase the entropy of the water molecules surrounding it.

‘Fuzzy’ interactions

Disorder to order transitions are not necessary for IDPs to confer functionality. There is a growing number of examples where IDPs are involved in functional interactions while remaining in a disordered state [24]. Such interactions have been labeled with the term ‘fuzzy’ as they maintain a heterogenous conformational ensemble throughout their lifetimes. There exist various physical mechanisms by which fuzziness, or disorder, in binding interactions confers advantages to protein function. For example, binding interactions between an IDP and a target protein where the IDP is able to form alternate contacts with its binding target can help reduce the entropic cost of binding, as well as control the accessibility of different sites on the protein for modulating interactions with different targets. [10, 8] IDPs can also play a role in interactions without making direct contacts with the binding partner. IDPs can act as flexible linkers for folded domains [3], or as ‘antennae’ for [?] recruiting further interactiors and stabilizing the binding of folded domains through long range interactions [31, 30]

It is becoming increasingly evident that nature is able to harness disorder as an adaptive mechanism for control in protein-function. Flexibility in conformational state allows cellular processes to greatly expand the functional repertoire of proteins by allowing for rapid switch-like control over interactions, expanding the functional repertoire of proteins, and fine-tuning the kinetics of interactions. It is due to all of these various physical mechanisms that the cell is able to carry out its complex tasks with such robustness and precision. Advances in this field have caused us to reconsider the ‘one structure, one function’ paradigm that has prevailed in structural

biology for decades. However, this remains a relatively novel area of structural biology, and there still remain many unsolved physical mechanisms in IDPs.

1.3 IDP function in the mitotic spindle

In this section we will address the role of IDPs in controlling the function of the mitotic spindle. The mitotic spindle is a complex molecular machine composed of microtubules, force generators, chromosomes, and numerous effector molecules which act in a coordinated manner to accomplish the process of chromosome segregation during cell division [14]. This process ensures that genetic material is transferred from the mother to the daughter cell in a timely manner and without errors which would in most cases result in lethality. Because cell division is a fundamental task in every cell's lifetime, mitotic spindles share common design features throughout eukaryotes [18]. The task of properly arranging and segregating chromosomes is effected ultimately by filament-like polymers known as microtubules which attach to chromosomes and physically pull the DNA to the daughter cell. In order to study the underlying mechanisms at play, we work with the mitotic spindle of the budding yeast *Saccharomyces cerevisiae* due to its minimal, yet highly conserved construction.

1.3.1 Microtubules

Microtubules are constructed of alternating pairs, or dimers, of the globular proteins α and β Tubulin. A cylindrical arrangement of tubulin dimers results in the formation of a rigid tube-like structure known as a microtubule. By growing, or polymerizing, and shrinking, depolymerizing, microtubules can effect force on a target [6]. Microtubules are involved in a number of other functions, such as serving as roadways along which transport molecules can carry cargo, and forming

the structural backbone of the cell. The spontaneous assembly of tubulin dimers in solution into a microtubule is heavily disfavoured. However, when free floating tubulins encounter pre-formed ring of tubulin molecules, the growth of a microtubule is greatly facilitated [12]. In cells, this template is known as the γ -Tubulin Ring Complex (γ -TuRC) which is a ring-like assembly of γ -Tubulin molecules held together by various other proteins known as γ -tubulin ring proteins (GTRPs). γ tubulin shares a similar structure to α and β tubulin and have been shown to act as nucleation templates for microtubules when assembled in a ring complex [17]. Furthermore, structural rearrangements of the γ -TuRC have been shown to either facilitate and inhibit nucleation [16].

1.3.2 γ -Tubulin & the γ -CT

For many years, microtubule nucleation was thought to be the sole function of γ tubulin. This view began to change after a mass spectrometry study published in 2001 of the yeast γ -Tubulin showed that the protein is phosphorylated *in vivo* at 8 sites. Several functional studies following up on the finding that γ -tubulin is regulated show that mutations altering phosphorylation sites, all of which lie in IDRs, have consequences on the organization and stability of microtubules but no effect on their nucleation. This opens a relatively unexplored field of functional coupling where the γ -TuRC acts not only as a microtubule nucleator, but as a signal integration hub for regulating downstream events in microtubule organization.

One of the best studied phosphorylation sites in γ -Tubulin is the heavily conserved Tyrosine (Y) 445 which lies in the disordered carboxyl terminal tail of γ -Tubulin (γ -CT). The γ -CT is defined as the final 35 residues in the C-terminal

portion of γ -Tubulin, which lie outside of the folded globular domain. The γ -CT has been shown to be essential for survival in *S. cerevisiae* when cleaved [26]. Substitution of an Aspartic Acid (D) residue in the place of Y445, making the Y445D mutant, results in slow growing cells with unstable and misaligned mitotic spindles [25]. The aspartic acid substitution is used as a controllable means for recreating the electrostatic environment of a phosphate group by introducing a negative charge. These findings suggest that γ -Tubulin is playing a role outside of its canonical function of nucleation and is coordinating the dynamics of the mitotic spindle. However, very little is known about the interactions and physical mechanisms that phosphorylation at Y445 affect. The coupling of post-translational modifications (PTMs) to the C-terminal tails of tubulins is well described in the γ -tubulin orthologues α and β tubulin. Specific combinations of PTMs on the tubulin tails act as a ‘tubulin code’ for selectively recruiting motor proteins and microtubule associated proteins to the microtubule lattice. A similar code has not yet been described for γ -Tubulin despite evidence that it is regulated *in vivo*. While the functional importance of phosphorylation and IDRs in γ -Tubulin is becoming increasingly clear, the physical mechanisms by which local modifications at IDRs can have global impacts on the large molecular machine remain unstudied.

1.4 Experimental question

We hypothesize that the addition of a negative charge at the position Y445 (Y11 for the polypeptide in isolation) in the γ -CT alters the conformational sampling of the disordered tail in such a way as to be able to regulate the function of the complex.

1.5 Approach

In order to detect the rapid changes in conformational sampling, we use a powerful computational technique known as Molecular Dynamics (MD) simulations. We will be simulating the dynamics of two forms of the γ -CT: WT, and Y11D. We will perform simulations on the γ -CT in isolation as well as in the presence of the entire γ -Tubulin protein.

CHAPTER 2

Theory & Methods

Life can only be understood
backwards; but it must be lived
forwards.

Søren Kierkegaard

The main technique we will use to study the behaviour of IDPs is the computational technique of Molecular Dynamics (MD) simulations. IDP dynamics are shaped by various types of physical interactions acting on a high number of conformational degrees of freedom all on a very fast timescale. For this reason it is difficult to predict the dynamics of IDPs *ab initio*. MD is a brute-force approach which iteratively solves the equations of motion for every interaction in a system of atoms in 3D space. What results is a trajectory in space and a velocity for every atom in the system in time which we can use to visualize the conformational sampling of our IDP of interest and compute thermodynamic quantities. While this can be a computationally demanding task, it is currently the most reliable way of computationally studying the dynamics of molecular systems. We will use this approach to study the conformational dynamics of two isoforms of the γ -CT: WT, and Y445D.

2.1 Molecular Dynamics Simulations

We represent our system as a set of N atoms represented as vectors $R = \{\mathbf{r}_1, \mathbf{r}_2, \dots, \mathbf{r}_N\}$ in three dimensional space. We then use classical Newtonian mechanics to obtain the changes in position of the particles as a function of time. For a peptide in solution, this would consist of the atoms in the peptide, and water atoms and the forces arising from interactions between all the particles in the system.

2.1.1 Computing trajectories of atoms

The central principle of MD is that the potential energy arising from interacting particles is a function of their positions in space. Since force is related to potential energy, it follows that the acceleration of the particles is a function of the potential energy, and so the motion of the particles can be obtained. Given a description of the potentials arising from interactions between the different atoms, which we call a force field, we can iterate through every atom in the system and calculate the force that would arise as a function of the potential energy function. The potential energy given by the force field can be written as $V(\mathbf{r}_1, \mathbf{r}_2, \dots, \mathbf{r}_N)$ is a function of the positions of each atom. Using the classical definition of force as $\mathbf{F} = m\mathbf{a}$, we can combine the positions of each atom with the force field to compute the force acting on each atom as follows.

$$\mathbf{F}_i = -\frac{\partial V(\mathbf{r}_1, \mathbf{r}_2, \dots, \mathbf{r}_i, \dots, \mathbf{r}_N)}{\partial \mathbf{r}_i} \quad (2.1)$$

Given that the force on an atom is the result of interactions with all other atoms fix this in the system, we obtain the force on a particular atom as the sum of the force of the interactions with all other atoms j in the system. So we get $\mathbf{F}_i = \sum_j \mathbf{F}_{ij}$ Given

the total force on an atom, we can compute its trajectory in space by numerically integrating Newton's equations of motion. This process is repeated and trajectories are stored and updated for the desired number of steps in the simulation.

$$\frac{\partial^2 \mathbf{r}_i}{\partial t^2} = \frac{\mathbf{F}_i}{m_i} \quad (2.2)$$

2.1.2 Force Field

The functions for potential energy of every type of interaction in the system are defined in what we call a force field. The energy between two interacting atoms can be broken down into two broad types of interactions: bonded and non-bonded interactions.

$$E_{total} = E_{bonded} + E_{nonbonded} \quad (2.3)$$

The bonded energy term can be written as the sum of energies arising from the bond itself (E_{bond}) which is a function of the bond length, the potential arising from the angle formed by the bond (E_{angle}), as well as the torsional/dihedral angle ($E_{dihedral}$) arising from the rotation of three bonds about two intersecting planes.

Non-bonded interactions can have two contributing factors; electrostatic force, and van der Waals force. The electrostatic potential ($E_{electrostatic}$) arises from the interaction of the charges of particles, while the van der Waals potential ($E_{vanderWaals}$) arises from the attraction or repulsion between uncharged groups. In most systems, non-bonded interactions by far outnumber bonded interactions and thus carry most

of the computational weight in an MD simulation. in m Combining all of these terms, we can write the full description of forces in the system as:

$$E_{total} = E_{bond} + E_{angle} + E_{dihedral} + E_{vanderWaals} + E_{electrostatic} \quad (2.4)$$

should i include
this?

$$E(r_N) = \sum_{bonds} K_r(r-r_0)^2 + \sum_{angles} k_\theta(\theta-\theta_0) + \sum_{dihedrals} K_\phi(1+\cos(n\phi-\delta)) + \sum_{i,j} \{4\epsilon_{i,j} \frac{\sigma_{ij}}{r_{ij}}\} \quad (2.5)$$

The MD algorithm evaluates $E(r_N)$ at every time step to obtain the force on each atom and therefore the trajectory at each time step. Given such a fine-grain level of modelling, this process is the most time costly step in an MD simulation. However, an important advantage to such a low level description of the system is that more complex phenomena such as the hydrophobic effect and hydrogen bonding which are known to be essential to protein dynamics do not need to be coded explicitly in the models. Instead, they arise naturally from this definition of the system.

Another key component to the force field, is the definition of parameters for the different types of interactions and particles in the system. Parameters can include values for charge, mass, bond length, etc. These are often obtained from experimental measurements. The force field must naturally also contain a set of definitions for the various types of atoms and functional groups it can model. Therefore, the choice of force field can have important consequences on the outcome of the simulations and must be chosen with care.

2.1.3 Preparing the system

The starting point of an MD simulation is a force field and a set of initial coordinates for the system of interest. Before a simulation can be successfully run, there are several pre-processing steps that must be executed.

As mentioned earlier, hydrogen bonding and the hydrophobic effect play very important roles in shaping the dynamics of polypeptides therefore our model must include water molecules. We therefore place the peptide atoms are placed in a simulated box where water molecules are introduced to fill the remaining space. All subsequent force calculations in MD will consider interactions between solvent-solvent and solvent-peptide atoms. Given that many more water molecules will be present than peptide molecules, computations on solvent atoms are computational costly. Some variations on MD avoid these computations by modelling the solvent implicitly as a mean field instead of explicitly considering every atom in the system.

Once the peptide is solvated any initial steric clashes between atoms must be allowed to relax. Typically this involves executing an energy minimization algorithm which searches for atomic coordinates that minimizes the forces between atoms to move the system towards an energy minimum. No minimization algorithm guarantees convergence to a global minimum in finite time on a realistic system. However, convergence to a local minimum is often sufficient to eliminate significant clashes.

At this point, we could begin an MD simulation and obtain trajectories in the NVE ensemble (constant number of particles, volume, and energy). However, we are often interested in comparing results from MD to experimental measurements such as those from NMR where the system is under constant temperature and pressure.

It is therefore necessary to ensure that the forces in the system don't produce large fluctuations in the pressure and temperature of the ensemble. In order to keep the temperature constant and achieve an NVT (constant number of particles, volume, and temperature) we use a thermostat. Since the temperature of a system is a function of the kinetic energy, a thermostat re-scales the velocities of the atoms in the system to achieve a given temperature. Likewise, for maintaining constant pressure, a barostat adjusts the size of the box to counteract fluctuations in pressure and thus achieving an NPT ensemble (constant number of particles, pressure, and temperature). During the equilibration step, we first let the system equilibrate to the desired temperature by executing a short simulation in NVT. Then under NPT we allow the system to adjust to the desired pressure. Once both equilibration simulations are complete, the system is ready for a full simulation in NPT.

2.2 Trajectory Analysis

The MD simulation generates a set of coordinates for every atom in the system as a function of time, $r(t)$. From these trajectories we can compute several quantities to study conformational changes in the peptide over time.

2.2.1 Root Mean Square Deviation

We measure the square displacement between the coordinates of atom i at time t weighted by the mass of the atom m_i . We iterate this process for every atom in the peptide to obtain a measure of the degree of change between two conformations in time.

$$\text{RMSD}(t_1, t_2) = \left[M^{-1} \sum_{i=1}^N m_i ||\mathbf{r}_i(t_1) - \mathbf{r}_i(t_2)||^2 \right]^{\frac{1}{2}} \quad (2.6)$$

2.2.2 Radius of gyration

The radius of gyration is a measure of a structure's compactness. To obtain the radius of gyration, we compute the mean squared distance from every atom r_i to the molecule's centre of mass r_{mean} .

$$R_g(\mathbf{r}) = \sqrt{N^{-1} \sum_{k=1}^N (\mathbf{r}_k - \mathbf{r}_{mean})^2} \quad (2.7)$$

2.2.3 Diffusion coefficient and Hydrodynamic Radius

Like radius of gyration, diffusion coefficient is a proxy for the compactness of a macromolecule. Unlike radius of gyration, diffusion coefficient can be measured through NMR spectroscopy and thus allows us to make direct comparisons between simulation trajectories and experimental values. The translational diffusion coefficient of a macromolecule is defined as the rate at which its center of mass is able to diffuse through a solvent of given viscosity under a certain hydrodynamic model. Conformations with high diffusion rates experience rapid displacement of their center of mass, while conformations with greater friction force with the solvent experience reduced diffusion coefficients.

The process of computing the translational diffusion coefficient for a particular conformation is done by the software package `hydroNMR`. The method of calculating the diffusion coefficient will not be discussed here in detail as it is beyond the scope of this work.. The main concept is that the software models each atom in a list of atomic coordinates, in our case obtained by MD, as a spherical bead. This chain of beads is packed with a hexagonal lattice and internal beads are removed to extract

a topology of residues exposed to the solvent. From this topology, the software calculates the frictional force that a given conformation would exert on the solvent, this is contained in the translational friction tensor Ξ . The following expression gives us the translational diffusion tensor \mathbf{D}_t .

$$\mathbf{D}_t = k_B T \Xi_t^{-1} \quad (2.8)$$

Where k_B is the Boltzmann constant ($1.380 \times 10^{-23} \text{ m}^2 \text{ kg s}^{-2} \text{ K}^{-1}$) and T is the temperature in Kelvin. The trace of the translational diffusoin tensor is invariant regardless of the molecule's orientation and is thus used to define the translational diffusion coefficient D_t .

$$D_t = \frac{1}{3} \text{tr}(\mathbf{D}_t) \quad (2.9)$$

Knowing D_t , we can use the Stokes-Einstein equation to obtain an expression for the effective hydrodynamic radius which measures the diffusion of spherical particles.

$$r = \frac{k_B T}{6\pi\eta D_t} \quad (2.10)$$

Where r is the hydrodynamic radius and η is the viscosity of the solvent.

2.2.4 Covariance Analysis

When analyzing MD trajectories, we are often interested in observing collective motions. This is because global motions are likely to be involved in some functional mechanism. However, molecular trajectories typically feature complex motions along many axes and time scales which can often make it difficult to detect coordinated

motions. For example, local rearrangements, vibrations, rotations, and random diffusion are examples of non-coordinated motions that likely do not contribute to a functional mechanism. The goal in MD trajectory covariance analysis is to obtain the axes of motion where atoms in the peptide of interest show a high degree of correlation which could be indicative of a global coordinated motion.

Covariance analysis, or principal component analysis is a mathematical tool which isolates principal axes, or components of motion by computing the covariance between atoms at every time point in the simulation. We compute the covariance for all N atoms in 3 dimensions, resulting in a covariance matrix of size $3N$.

$$C_{ij} = \left\langle M_{ii}^{\frac{1}{2}}(\mathbf{x}_i(t) - \langle \mathbf{x}_i(t) \rangle) M_{jj}^{\frac{1}{2}}(\mathbf{x}_j(t) - \langle \mathbf{x}_j(t) \rangle) \right\rangle \quad (2.11)$$

The eigenvectors of the covariance matrix, C define the set of orthogonal axes along which maximize variance. Note that $\langle \cdot \rangle$ denotes a time average. Due to the constraints imposed by the backbone, only a couple of eigenvectors are expected to contribute most to global movements.

$$R^T C R = \text{diag}(\lambda_1, \lambda_2, \dots, \lambda_{3N}) \quad \text{where} \quad \lambda_1 \geq \lambda_2 \geq \lambda_{3N} \quad (2.12)$$

Where R is the transformation matrix whose columns contain an eigenvector. Using this matrix to diagonalize C , we get a diagonalized C containing the set of eigenvalues λ_i for every eigenvector in R along its main diagonal. The magnitude of the eigenvalue tells us the amount of variance captured by its corresponding eigenvector and can thus be used to guide our projection toward the major axes of motion.

If we wish to visualize the system's motions along a particular axis and filter out motions along other axes, we can project the coordinates of each atom along an eigenvector. We can the following transformation to obtain the new set of coordinates $\mathbf{p}(t)$.

$$\mathbf{p}(t) = R^T M^{\frac{1}{2}} \mathbf{x}(t) \quad (2.13)$$

The resulting trajectory lets us visualize motions along any component and is a useful tool for detecting coordinated structural changes. Another useful application of the covariance matrix is for comparing the structural sampling of major modes in two different trajectories. Such comparisons can be used to assess the convergence of sampling, as well as for detecting major changes in conformational sampling. We define a quantity known as the subspace overlap which corresponds to the degree of similarity between two trajectories along their major components. This problem is equivalent to comparing two matrices of eigenvectors and the space that they span and so the subspace overlap is defined as follows:

$$\text{overlap}(\mathbf{v}, \mathbf{w}) \equiv \frac{1}{n} \sum_{i=1, j=1}^{n,n} (\mathbf{v} \times \mathbf{w})^2 \quad (2.14)$$

$$d = \sqrt{\text{tr}((\sqrt{C_1} - \sqrt{C_2})^2)} \quad (2.15)$$

$$\text{normalized overlap}(C_1, C_2) = 1 - \frac{d}{\sqrt{\text{tr}(C_1) + \text{tr}(C_2)}} \quad (2.16)$$

CHAPTER 3

Conformational analysis of the γ -Tubulincarboxyl terminus

Only in disorder are we conceivable.

Roberto Bolaño

In this chapter we discuss the impact of phosphorylation on the global dynamics of the γ -TubulinC-terminus (γ -CT). We begin from the facts that the γ -CT has been shown to be phosphorylated *in vivo* [15], and that altering the phosphorylation status of the γ -CT modulates the dynamics of the mitotic spindle [25]. We therefore hypothesize that phosphorylation at the γ -CT IDP is acting to regulate spindle dynamics via a structural mechanism. More specifically, we will be studying the highly conserved Tyrosine 445 (Y445) of the γ -CT which has been identified as a key phospho-site in this system [25].

In order to understand the effect of phosphorylation at Y445, we study the conformational sampling of non-phosphorylated and phosphorylated forms of the γ -CT. Because phosphorylations are difficult to implement controllably *in vivo* and *in vitro*, we approximate the electrostatic effects of a phosphorylation by introducing an acidic residue, Aspartic Acid (D), at the phosphorylation site. We therefore study the wild-type sequence, WT: LLRGAAEQDSYLDLVDDENMVGELEEDLDADGDHKLV, and the phospho-mutant Y445D: LLRGAAEQDSLDLVDDENMVGELEEDLDADGDHKLV using MD simulations. By comparing results from our simulations to experimental measurements previously performed with NMR spectroscopy on the γ -CT, we are

able to propose that local changes in charge at the 445 residue in the polypeptide modulate the conformational sampling of the γ -CT. The changes in conformational sampling we observe point to a physical mechanism for regulating the availability of binding surfaces on γ -Tubulin. Furthermore, we describe a novel mode of IDP control whereby functionality arises from switch-like transitions that lie entirely within disordered states.

3.1 NMR

Our starting point comes from NMR experiments done by collaborators in the Department of Chemistry at McGill on the WT and YD forms of the γ -CT. Through protein NMR spectroscopy we are able to obtain accurate *in vitro* measurements of the structural and dynamic properties of polypeptides. Among these are secondary structure state, dynamic conformational changes, and structural properties such as diffusion rates. Given that the γ -CT is intrinsically disordered and therefore highly dynamic, this makes NMR a particularly well suited to this problem. Diffusion measurements show that the major conformation of both forms corresponds to that of a collapsed polypeptide. By computing the effective hydrodynamic radius of the polypeptides using the Stokes-Einstein ?? we can compare the compactness of the γ -CT to other known structures. The for WT we obtain $D_t = 1.25 \times 10^{-6} \pm 1 \times 10^{-8} \text{ cm}^2 \text{ s}^{-1}$, $r = 14.2 \text{ \AA} \pm 0.2$ and $D_t = 1.224 \times 10^{-6} \pm 3.503 \times 10^{-8} \text{ cm}^2 \text{ s}^{-1}$, $r = 15.6 \text{ \AA} \pm 0.2$ for the YD mutant. Both are close to the hydrodynamic radius of the folded fibronectin binding protein D3 ($r = 14.9 \text{ \AA}$) [27] and well under the predicted Stokes radius of an extended 39 amino acid chain . This is a surprising ref nmr fig finding given the high content of negatively charged residues (15 of 39 residues) in

both forms would be expected to promote open conformations. However, because that the γ -CT also has a relatively high number of hydrophobic residues (14/39), it is likely that there are other forces, such as the hydrophobic effect, acting on the packing of the peptide. We also note that the YD has a slightly higher Stokes radius than the YD suggesting some shifts in conformational sampling that are absent in the WT. Chemical shift secondary structure predictions show that both forms occupy a disordered random coil state and do not show evidence of adopting any secondary structure domains. Therefore, we do not observe any disorder-order transitions which are common in functionally-coupled phosphorylated IDPS. However, relaxation-dispersion experiments, which detect changes in the chemical environment of residues on the micro-millisecond timescale, show that the Y445D mutant undergoes large coordinated transitions, while the WT dispersion profile is flat. Combining the dispersions brought about by the YD mutation with the shift in global D_t to more open conformations, we hypothesize that the YD mutation induces collective motions between a collapsed major state and an extended minor state.

In this work we use MD simulations of both γ -CT forms to gain further insight into the transition hypothesized by NMR.

insert nmr figs

3.2 Setting up the MD runs

Molecular Dynamics simulations (MDS) on WT and Y445D γ -CT were carried out using MPI-enabled GROMACS 4.6.6 software[?] and a CentOS 5 high performance computational cluster. Calculations were distributed over 64 Dual Sandy

Bridge 8-core, 2.6 GHz computing nodes and run under periodic boundary conditions with the OPLS-AA (Optimized Potential for Liquid Simulations All Atom) force field [?]. The starting γ -CT polypeptide configurations were obtained from secondary and tertiary structure predictions by RaptorX [?] and solvated using the SPCE (extended single point charge) water model in a dodecahedral box while enforcing a minimum distance between the edge of the box and solute of 1 nanometer. The total charge of the system was neutralized by adding sodium ions to the solution. Energy minimization was carried out using a steepest descent algorithm for a maximum of 50,000 steps until a maximum force of 100 kJ/mol between atoms was achieved. A 1 nm cut-off was used for non-bonded interactions, and long-range electrostatics were calculated using a Particle Mesh Edwald Sum algorithm. The systems equilibrated under the constant NVT and NPT ensembles (288K and 1 atm) for 5 ns before the production 2 μ s simulations. Post-processing of all trajectories was done using the `trjconv` module of GROMACS. Theoretical random-coil structural ensembles (10,000 conformers) were calculated based on the γ -CT primary amino acid sequence using Flexible Meccano software [?]. Translational diffusion coefficients were calculated for each structure using hydroNMR software [5]. MD conformations were grouped into percentile classes based on radius of gyration (R_g) computed using the GROMACS `g_gyrate` module. Each R_g percentile group was represented by the three structures with lowest root-mean-squared-difference RMSD values to all other structures, calculated using the GROMACS `g_rms` module. Atomic distance matrices were calculated using the GROMACS `g_mdmat` module.

3.3 Conformational sampling of γ -CT isoforms

We computed atomic trajectories for the WT and YD forms of the γ -CT in all-atom MD simulations with durations of 2 μ s. From the resulting trajectories we are able to capture dynamics and conformational sampling that are remarkably consistent with those measured in NMR.

γ -CT does not adopt any stable secondary structure

The first question we addressed was whether the structures in our MD trajectories feature the same lack of global structure that was observed in NMR. We used the `dssp` algorithm [13] in the VMD software package [11] to compute secondary structure assignments on each residue in the chain. Assignments by `dssp` are based on computations of hydrogen bonding energies between all atoms. Since hydrogen bonds are the primary stabilizing interaction that gives rise to backbone secondary structure, `dssp` is able to classify geometries arising from potential hydrogen bonds to a category of secondary structure motif found in a large database of annotated structures. We apply this algorithm to every frame in the trajectories at 1 ns intervals to assess secondary structure motifs at every residue as a function of simulation time **Fig. 3–1**. Apart from some local helicity in the middle residues, secondary structure assignment plots for all four trajectories point to a consistent absence of global secondary structure motif. The major classes of secondary structure present are turn and coil geometries which correspond to a largely unstructured ensemble of conformations.

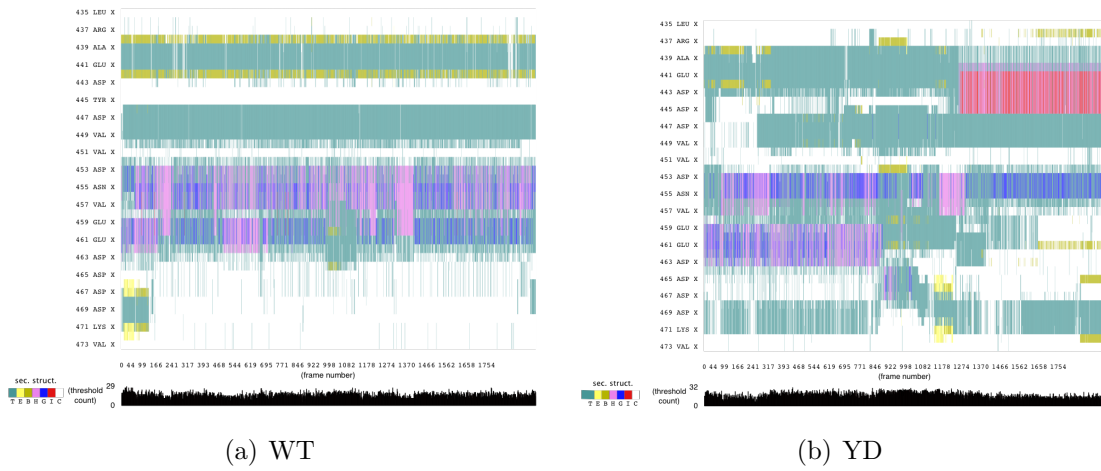


Figure 3–1: γ -CT Secondary Structure Assignments

Per-residue secondary structure assignments based on 3D coordinates are computed for every frame of the simulation. WT and YD trajectories lack global and persistent secondary structure motifs throughout the duration of the simulation.

Apart from turn motifs and small local α -helices, the γ -CT samples largely disordered conformations and does not undergo any disorder-order transitions. T: turn, E: extended, B: isolated bridge, H: α -helix, G: 3/10 Helix, I: π -helix, C: coil.

Although we do not observe ordered secondary structure rearrangements by looking at `dssp`, we compute RMSD to ask whether the simulations produce any conformational changes in the disordered ensemble. RMSD quantifies the distance between superimposed structures and is therefore a useful tool for detecting the presence of conformational changes in a trajectory. We therefore computed backbone RMSD values for every frame in the simulation with respect to the starting structure. Since the starting conformation is not derived from experimental data and is not expected to correspond to a native state, we also compute RMSD with a 10ns sliding window where every frame is compared with the one 10ns before. In the middle portion of the YD simulation, both methods of computing RMSD contain sharp peaks which indicate the presence of large scale backbone rearrangements **Fig. 3–2**. In contrast, WT RMSD values remain stable throughout the simulation. This suggests that the YD mutation can modulate conformational exploration and the stability of the γ -CT.

RMSD figs

γ -CT is largely collapsed

Given that NMR reports transitions between extended and collapsed conformations in the YD mutant, we hypothesize that a similar motion is driving the displacement observed in the RMSD computations. In order to obtain values of compactness that can be compared directly to NMR results, we compute the translational diffusion coefficient (D_t) of conformers in our simulations. As a reference point for interpreting the diffusion values of the trajectories, we use the software `flexiblemeccano` to compute an ensemble of disordered peptides of the YD polypeptide. `flexiblemeccano`

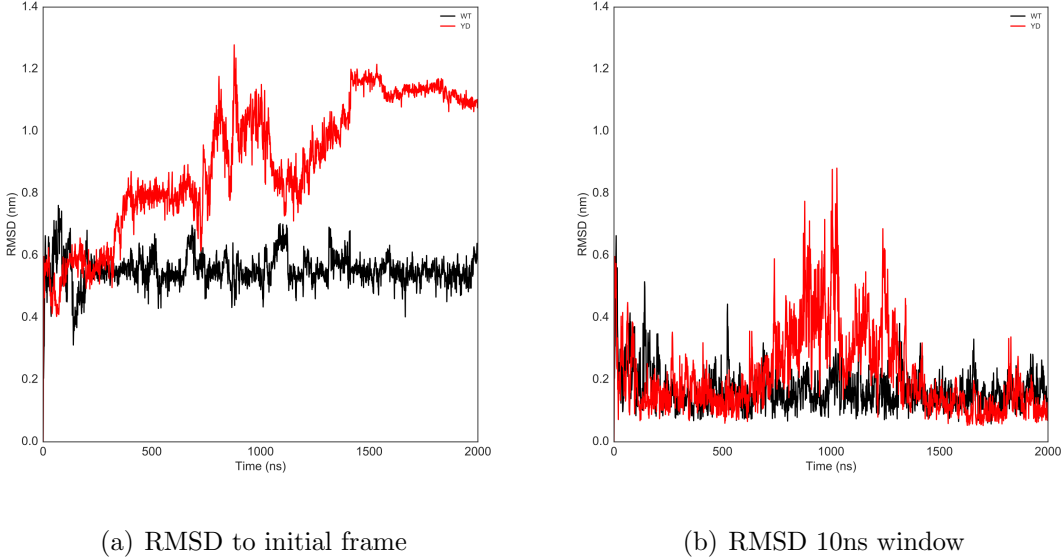
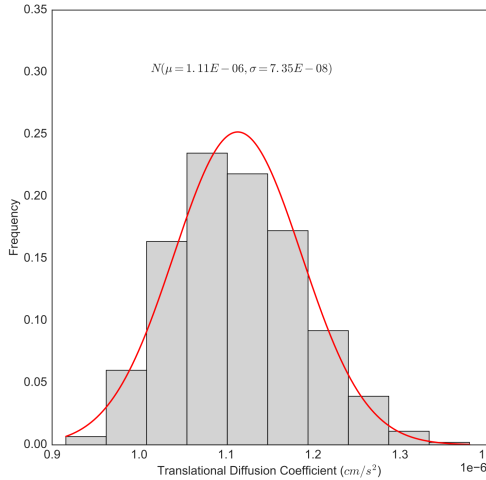


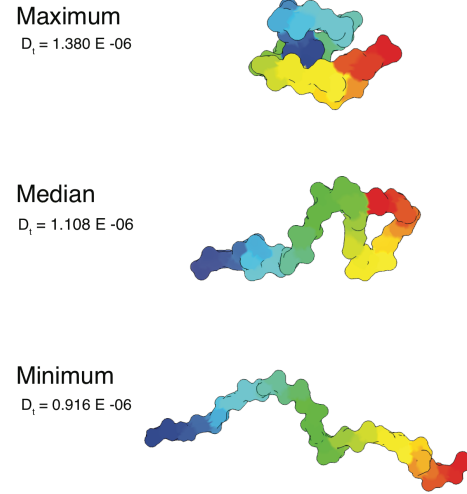
Figure 3-2: RMSD

takes a primary sequence as input and generates an ensemble of 3D conformations based on amino acid specific conformational potentials and volume exclusion. We then use hydroNMR to compute D_t values for each conformer and obtain a distribution for the D_t of the γ -CT. From this distribution **Fig. 3-3** we obtain a large range of conformations; from highly collapsed, to extended chains against which we can compare MD-derived values.

We computed global averages for the radius of gyration, and translational diffusion coefficient over the 2 μ s simulations. Both simulations appear to occupy largely collapsed conformations which agrees with experimental findings **Fig. 3-4**. The WT polypeptide D_t mean is $D_t = 1.237 \times 10^{-6} \pm 1.5816 \times 10^{-8} \text{ cm}^2 \text{ s}^{-1}$ while the value obtained through NMR is $D_t = 1.25 \times 10^{-6} \pm 1 \times 10^{-8} \text{ cm}^2 \text{ s}^{-1}$. Similarly to what was seen by NMR, we find that the mean D_t of the Y445D γ -CT polypeptide is



(a) Distribution of D_t in conformer ensemble



(b) Representative structures

Figure 3–3: γ -CT predicted conformational ensemble

We use **flexiblemeccano** to obtain a conformer ensemble based on the primary sequence of the γ -CT and plot D_t for every conformer in the set of 10,000 sampled structures **Fig. 3–3(a)**. We visualize the structures corresponding to the maximum, minimum, and median D_t . **Fig. 3–3(b)**

slightly lower than that of the WT γ -CT ($D_t = 1.224 \times 10^{-6} \pm 3.503 \times 10^{-8} \text{ cm}^2 \text{ s}^{-1}$).

These results confirm that the γ -CT, while disordered, is more compact than a fully denatured polypeptide chain, and that the YD γ -CT is more extended on average.

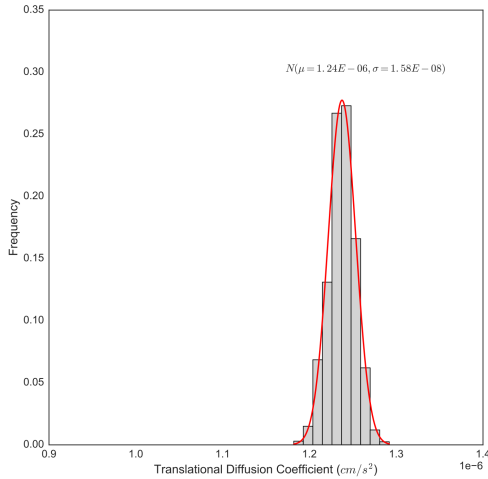
Translational diffusion coefficient measurements in NMR report that both γ -CT forms primarily occupy collapsed conformations. The global experimental average for the WT polypeptide obtained through NMR is $D_t = 1.25 \times 10^{-6} \pm 1 \times 10^{-8} \text{ cm}^2 \text{ s}^{-1}$ which agrees well with the NMR-derived value ($D_t = 1.25 \times 10^{-6} \pm 1 \times 10^{-8} \text{ cm}^2 \text{ s}^{-1}$).

chi square
goodness of fit
talk about
benchmark for
collapsed state

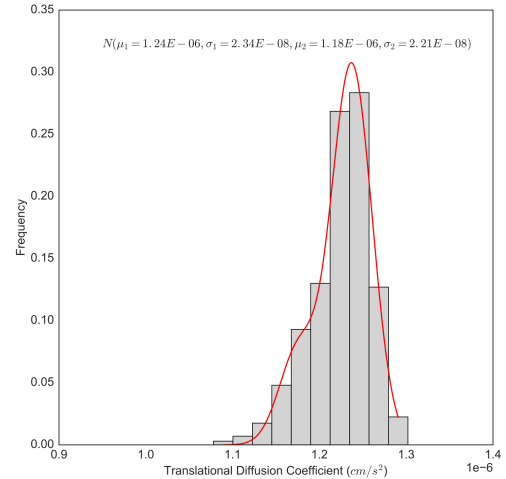
Similarly to what was seen by NMR, we find that the mean D_t of the Y445D γ -CT polypeptide is slightly lower than that of the WT γ -CT ($D_t = 1.224 \times 10^{-6} \pm 3.503 \times 10^{-8} \text{ cm}^2 \text{ s}^{-1}$). These results confirm that the γ -CT, while disordered, is more compact than a fully denatured polypeptide chain **Fig. 3–4(c)**.

Although both forms of the γ -CT primarily occupy collapsed and disordered conformations, we do observe that, as in NMR, the YD γ -CT has a slightly lower mean D_t than WT. From NMR we hypothesize that this is caused by transitions between compacted and extended driven by enhanced dynamics in the YD mutant. Lending support to this hypothesis, we show that we are able to explain the distribution of diffusion coefficients in the YD mutant as the sum of two gaussian distributions with parameters $\mu_1 = 1.24 \times 10^{-6} \text{ cm}^2 \text{ s}^{-1}, \sigma_1 = 2.34 \times 10^{-8}, \mu_2 = 1.18 \times 10^{-6} \text{ cm}^2 \text{ s}^{-1}, \sigma_2 = 2.21 \times 10^{-8}$ **Fig. 3–4(b)**. This suggests that the YD dynamics likely give rise to a two-state system where a minor state occupies extended conformations **Fig. 3–4(c)**. Meanwhile, the WT D_t distribution is best explained by a single normal distribution which suggests that the peptide occupies a single stable state which corresponds to the compacted portion of conformation space **Fig. 3–4(a)**.

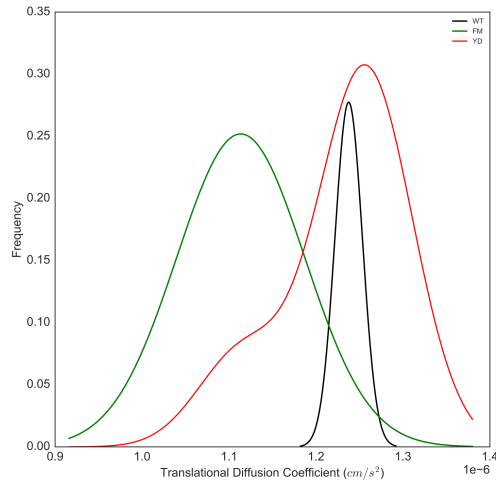
Looking at D_t as a function of simulation time, we found that the diffusion coefficient (D_t) of the WT γ -CT remains relatively constant throughout the simulation, ($D_t = 1.237 \times 10^{-6} \pm 1.5816 \times 10^{-8} \text{ cm}^2 \text{ s}^{-1}$ and agrees well with the NMR-derived value ($D_t = 1.25 \times 10^{-6} \pm 1 \times 10^{-8} \text{ cm}^2 \text{ s}^{-1}$). Similarly to what was seen by NMR, we find that the mean D_t of the Y445D γ -CT polypeptide is slightly lower than that of the WT γ -CT ($D_t = 1.224 \times 10^{-6} \pm 3.503 \times 10^{-8} \text{ cm}^2 \text{ s}^{-1}$). These results confirm that the γ -CT, while disordered, is more compact than a fully denatured polypeptide



(a) Figure A

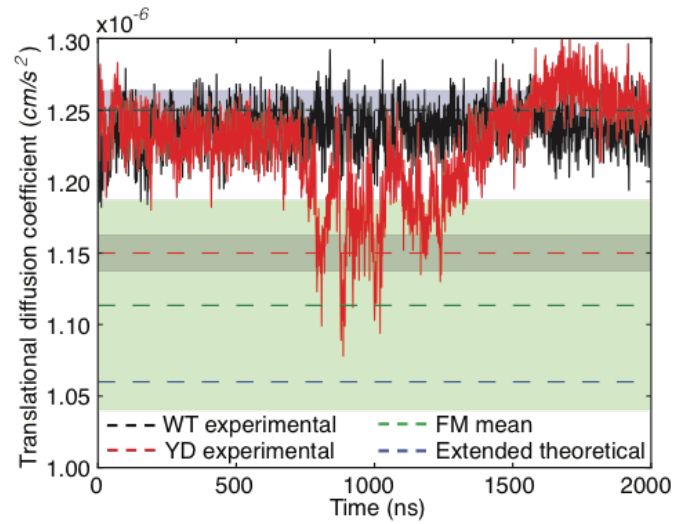


(b) Figure B

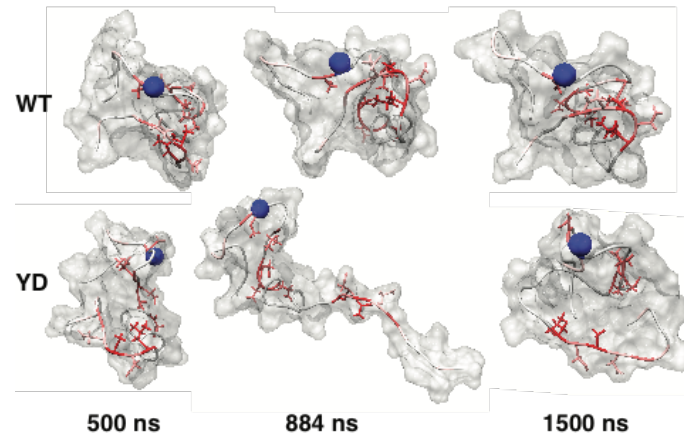


(c) Figure C

Figure 3–4: Distribution of diffusion coefficients



(a) D_t over simulation time



(b) Representative structures

Figure 3–5: Time-series plot of D_t over $2\mu\text{s}$ simulation.

chain. Interestingly, between 762 to 1255 ns in the MDS, the Y445D γ -CT underwent transient excursions to less compact conformations with significantly lower diffusion coefficients (mean $D_t = 1.152 \times 10^{-6} \pm 2.0325 \times 10^{-8} \text{ cm}^2 \text{ s}^{-1}$). This sub-population is more extended (i.e. diffuses more slowly) than any conformation sampled by the WT γ -CT throughout the entire MDS. While the Y445D γ -CT extended states do not overlap with the conformational ensemble of the WT γ -CT polypeptides, they do, however, lie close to the extended conformational space for a typical random-coil poly-peptide, as modeled by **flexiblemeccano** **Fig. 3–5**.

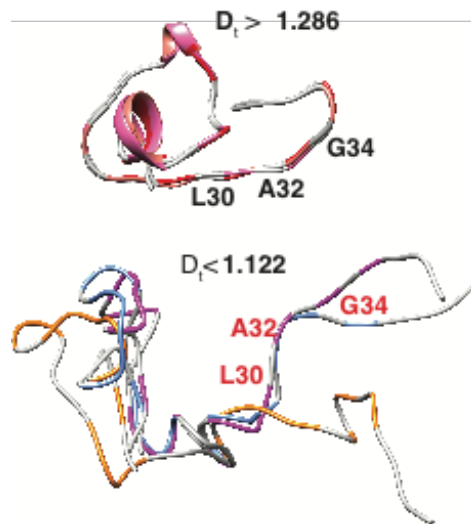
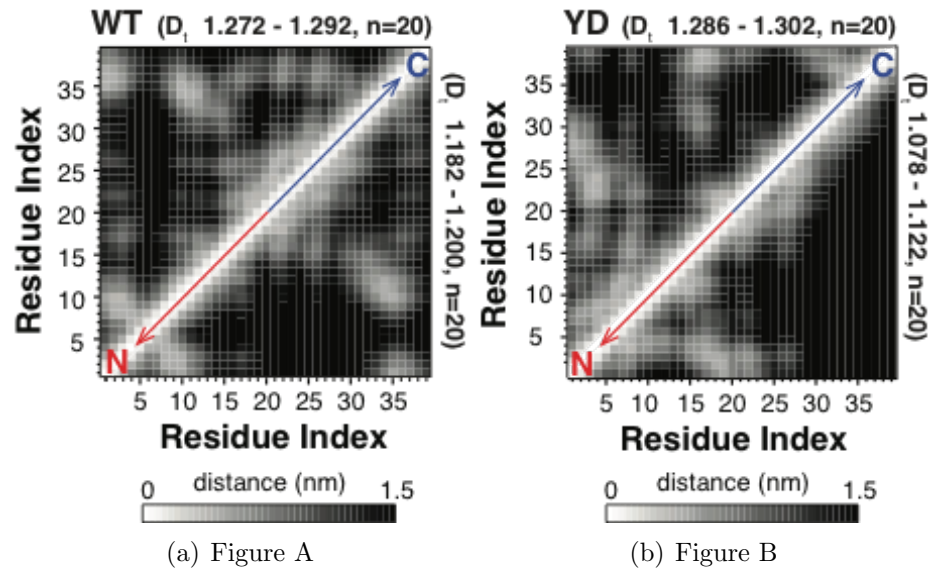
In order to visualize a non-overlapping subset of conformations to represent extended and collapsed states, we use the D_t distributions in **Fig. 3–4** to select the conformations within the top and bottom 1% (20 structures each) of the WT γ -CT and Y445D γ -CT. In the case of the WT, we do not expect the upper and lower D_t subsets to substantially differ, as the WT γ -CT conformations exhibit fairly homogeneous compactness overall. For Y445D γ -CT, we expect the upper D_t subset to resemble that of the WT γ -CT, while the lower D_t subset is expected to reflect the transient opening process. We plotted the mean distance between alpha carbons of all pairs of residues as contact maps for the set of collapsed (upper) and extended (lower) conformations of the WT γ -CT polypeptide **Fig. 3–6(a)** and the Y445D γ -CT polypeptide **Fig. 3–6(b)**. As expected, the upper and lower D_t subsets of the WT γ -CT and the upper D_t subset of the YD γ -CT polypeptides show similar patterns of pair-wise contacts. In contrast, the C-terminal residues in the lower D_t subset of the Y445D γ -CT lose the majority of contacts with N terminal residues, as

a consequence of the conformational expansion. Next, we isolated the three conformations from the upper and lower D_t subsets of Y445D γ -CT poly-peptides with the lowest all-to-all RMS, also known as centroid structures, shown in **Fig. 3–6(c)** with large relaxation dispersion magnitudes indicated in red. This analysis shows that the extended conformations consist of a compact N-terminus with residues located in the C-terminal region of the γ -CT, (including dynamically-broadened residues L30, A32 and G34) isolated from the N-terminus and solvent-accessible. Through MD we are able to re-produce the anomalously rapid diffusion (i.e. high compactness) of the WT and Y445D ground-state γ -CT polypeptides. Moreover, we saw that the YD substitution caused relatively slow collective motions of the entire polypeptide chain, as observed by NMR. This provides a possible explanation for how residues throughout a disordered polypeptide can experience a concerted, two-state, dynamical process presence of the Y445D mutation, and suggests that it is the separation of a cluster of residues located in N and C termini of the γ -CT polypeptide that drives a transition to extended conformations with a concomitant reduction of the translational diffusion coefficient.

3.3.1 Collective motions correspond to transitions between extended and collapsed conformations

Until this point, we have identified the presence of an extended sub-population of the YD γ -CT that is absent in the WT. This lends support to the hypothesis that the shift in D_t measured by NMR is due to transient expansions of the YD backbone into an extended state. Complementary to this finding, is the fact that residues in the YD polypeptide show evidence of collective motions detected as shifts in chemical environment through NMR. This suggests that the transition between

r2 figure ap-
pendix



(c) Figure C

Figure 3–6: Distribution of diffusion coefficients

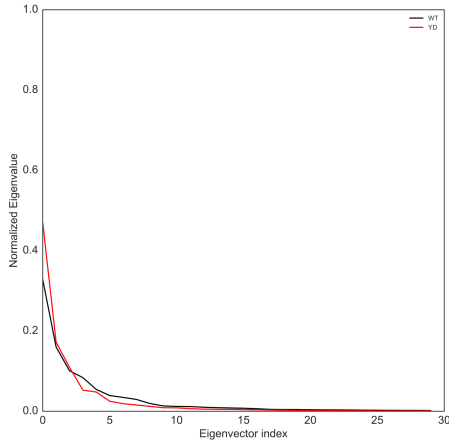


Figure 3–7: eigenvalues

states occurs in a coordinated manner. We therefore seek to test whether correlated motions are also present in the simulation, and if they are, whether they can explain the transitions between collapsed and extended states.

We performed covariance analysis, also known as Principal Component Analysis on γ -CT trajectories to identify major modes of correlated motion in our trajectories. We use `covar` and `anaeig` from the `GROMACS` package to build a backbone atom covariance matrix, extract principal modes, and perform dimensionality reductions through eigenvector projections. In order to eliminate rotational and diffusive translations which do not correspond to conformational motions, we align all frames in the trajectory to the average structure as computed by `covar` using RMSD based clustering. As is typical with molecular simulations which operate on a limited number of degrees of freedom, the first few eigenvectors in both trajectories account for nearly all of the variation in the trajectories **Fig. 3–7**.

look this up

add 3 PC component projection

time plot of projections in major components

We therefore focus our attention on the two first major modes of motion. **Fig. 3–8** shows a 2 dimensional projection onto the first two eigenvalues of WT and YD trajectories. Each point represents a 3D conformation in the 2 μ s simulation projected along the first two eigenvectors. The WT projection shows a conformational space that is closely clustered, indicative of constrained motions consistent with the low dispersions found in NMR, and the single state behaviour suggested by RMSD and D_t analysis. However, the YD appears to be exploring multiple conformation clusters which is in agreement with the presence of high dispersion groups found in NMR. Furthermore, by coloring each conformation with a normalized D_t value we are able to show that correlated motions along the major modes correspond with transitions between collapsed and extended states.

In order to visualize the transitions, we generate a porcupine plot depicting the direction of motion between conformations on two extremes of the second principal component projection **Fig. 3–9**. We show that the transition between collapsed and extended is indeed driven by a separation of the N and C terminus in a correlated fashion. With this analysis we are able to propose a physical mechanism to explain the concerted global dynamics and diffusion coefficient shift observed in NMR as the action of correlated motions brought about by a local change in electrostatic environment.

cosine content

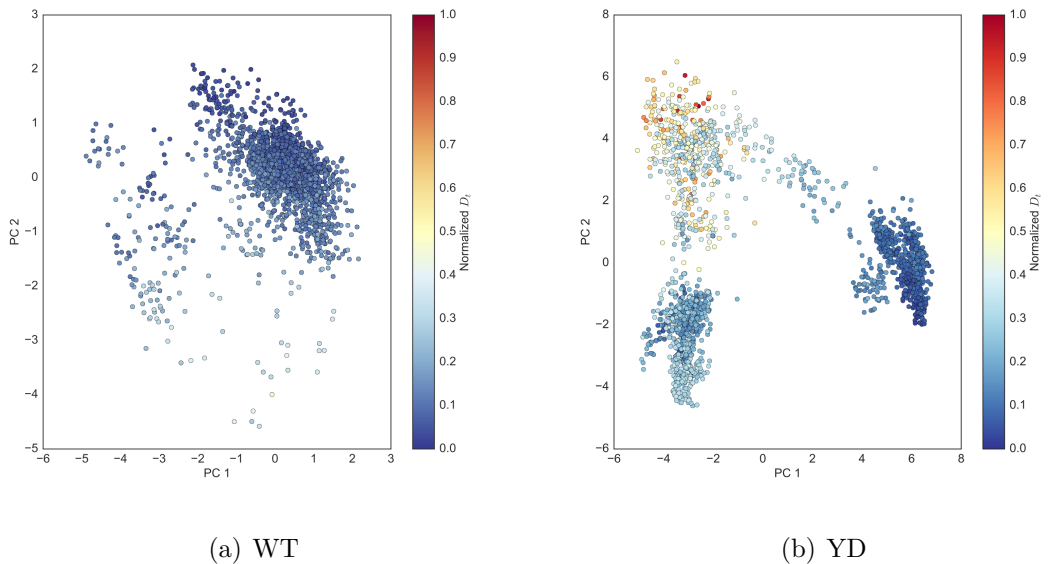


Figure 3–8: Principal Component Analysis
This is the text of the PCA figure

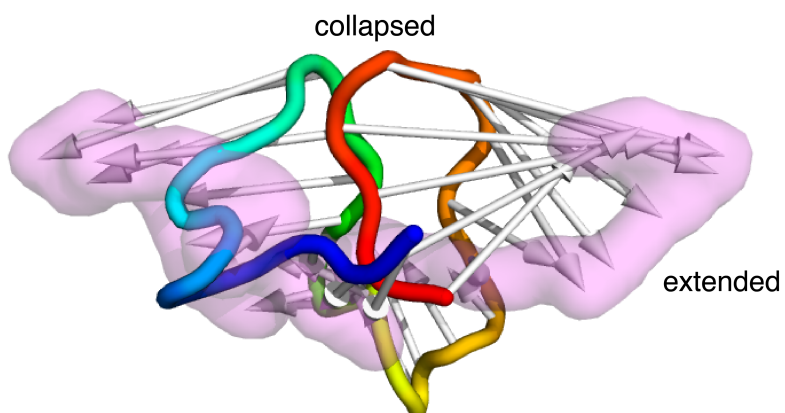


Figure 3–9: porcupine plot

3.3.2 Whole protein simulations and conserved properties of γ -CT

Our analysis of γ -CT structural properties using NMR and corresponding MDS are based on the WT and Y445D γ -CT polypeptides in isolation. In order to determine whether the conformations and dynamics we observed for the isolated γ -CT are physically consistent when attached to the full-length γ -Tubulinprotein, we docked the minimum D_t γ -CT model **Fig. 3–10** onto the globular domain of an S.c. γ -Tubulinhomology model as an initial structure for a whole protein simulation. Due to the substantial increase in system size, simulation times were reduced to 200ns. Despite the shorter simulation time, with the Y445D γ -CT polypeptide, the γ -CT in the whole protein simulation underwent exchange between extended and compact conformations **Fig. 3–10**, suggesting both states are still accessible in the presence of the globular domain. We found no contacts between residues in the globular domain with the 39 residues of the γ -CT throughout the 200 ns simulation (minimal distance between any pair of residues is ≥ 0.7 nm) . Structures for the full protein with the γ -CT at minimum radius of gyration (1.073 nm; model S11) and maximum radius of gyration (1.582 nm) are shown in Fig. 9A. This suggests that the γ -CT opening-closing mechanism can act independently of the rest of the protein.

glob contact
maps

Finally, we obtain evolutionary evidence that the physical mechanism of the γ -CT described here is likely present in many other organisms, and that it is not akin to other tubulin tails. We used the MUSCLE alignment tool [7] to generate multiple sequence alignments from sets of 71 β and 85 γ - CTs primary sequences spanning various eukaryotic kingdoms from the UniProt database [2] **Fig. 3–11**. We see from the resulting alignments that both CTs are enriched in acidic residues (Asp,

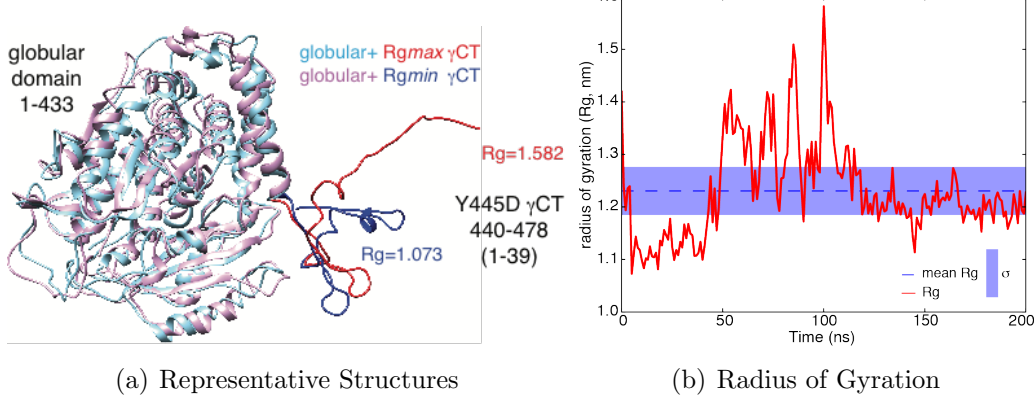


Figure 3–10: γ -Tubulin full protein simulation
This is the text

Glu). Whereas γ -CT across eukaryotes additionally contain clusters of hydrophobic or polar residues which are not found in α - or β -CTs. Interestingly, the residues most broadened in Y445D NMR spectra, i.e. those most affected by the compact-to-extended transition (V15, D19, E20, A32, G34), are all found in positions conserved either on a sequence level or on a physical property level (polarity/charge) in the consensus γ -CT sequence. We therefore hypothesize that clusters of hydrophobic residues, including those that contribute to transitions between compact and extended conformations in the S.c. Y445 γ -CT, are a conserved feature of an otherwise diverse set of γ -CTs across many eukaryotic organisms. Furthermore, given that the Y445 position is so pervasively conserved, it is likely that this mechanism of action is used by many other eukaryotes.

3.4 Discussion

Through NMR measurements and MD computer simulations, we demonstrate the first example of an IDP acting as a disorder-to-disorder regulatory switch, and

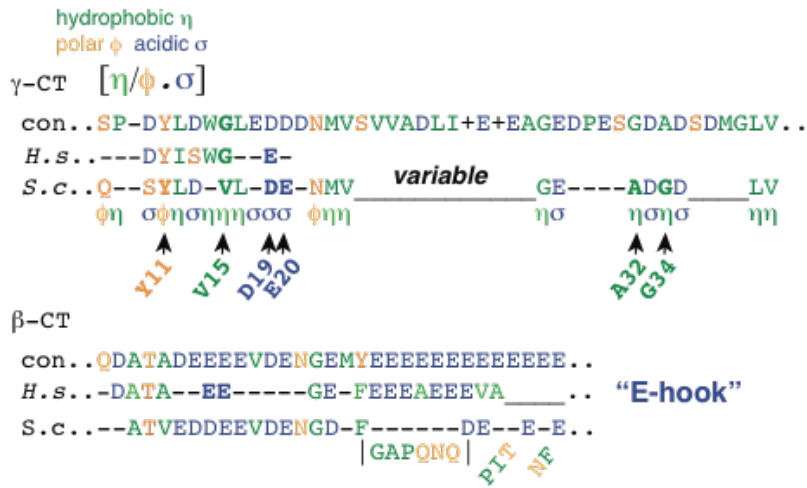


Figure 3–11: Multiple Sequence Alignment of γ -CT across eukaryotes

propose a physical mechanism to explain the regulation of an essential biological machine.

Both NMR and MD are in strong agreement that the conformational sampling of the γ -CT lies entirely within the disordered ensemble, as no signal of secondary structure was detected by either method. Diffusion measurements show that the major conformational state of the γ -CT in the WT and in the YD is collapsed, with the YD having a slightly larger hydrodynamic radius on average. However, NMR and MD simulations both provide evidence that a single point mutation to a negatively charged residue Y₁₁D produces concerted motions along the entire polypeptide that are not present in the WT γ -CT. Analysis of the collective motions detected in MDS by PCA correspond closely to transitions between collapsed and extended states which leads us to hypothesize that the changes in chemical environment detected in MDS and difference in hydrodynamic radius is a product of an correlated opening and closing motion brought about by the Y₁₁D mutation. This coordinated

opening is likely brought about by the effects of electrostatic repulsion as the Asp substituition introduces further negative charge in an already acidic region. It has been previously shown that charge has a strong influence on the conformational ensemble and diffusion rates in IDPs [19]. Once the γ -CT enters the open state, several hydrophobic residues in the middle of the polypeptide(L464, A466, G468) become accessible for protein-protein interactions.

Because both WT and YD appear to have the same collapsed native state and differ only when the YD undergoes transient excursion to an extended state, we can model such behaviour as a two well potential system **Fig. 3–12(b)**. The equilibrium between extended and collapsed conformations is shifted by phosphorylation to render extensions more accessible in the YD. Previously, such dynamics were only observed in the well characterized order-to disorder transitions, or the folding-on-binding paradigm [23]. Furthermore, this model stands in contrast to the existing view of disordered ensembles as uniform **Fig. 3–12(a)** spaces of random coils [21]. And instead, we observe that the disordered landscape has some structure that IDPs can selectively explore through PTMs to modulate functionality by giving rise to switch-like behaviour while still remaining disordered. Such behaviour likely presents advantages to the cell through its ability to provide high specificity and low affinity binding at a low entropic cost. This suggests for the first time that the disordered conformational landscape can be organized and can therefore be host to coordinated and functional transitions.

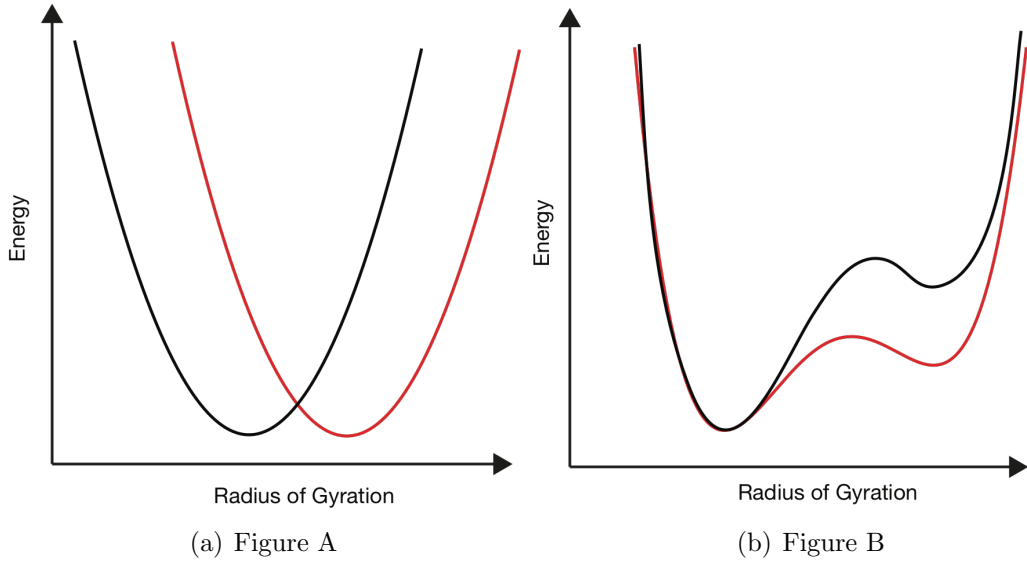


Figure 3–12: IDP Conformational Landscapes
Text

From these findings we propose that phosphorylation at Y445 of the γ -CT acts as a regulatory switch to modulate protein-protein interactions. In order to better visualize this mechanism, we dock 3D structures obtained from full γ -Tubulin simulations into cryo electron microscopy models of the γ -TuRC [16] **Fig. 3–13** which previously lacked any information on the γ -CT due to its disordered nature. Based on this visualization we can propose a mechanism to explain the phenotype of hyper-stable microtubules in the Y445D mutants *in vivo*. The extensions that project outward from the complex brought about by the YD substitution, or phosphorylation, allow the γ -TuRC to selectively recruit effector proteins to the minus end of microtubules, making them available to the entire complex to subsequently act in regulating microtubule dynamics. The constitutive addition of negative charge in the YD mutant therefore shifts the equilibrium between the collapsed and extended states, leading

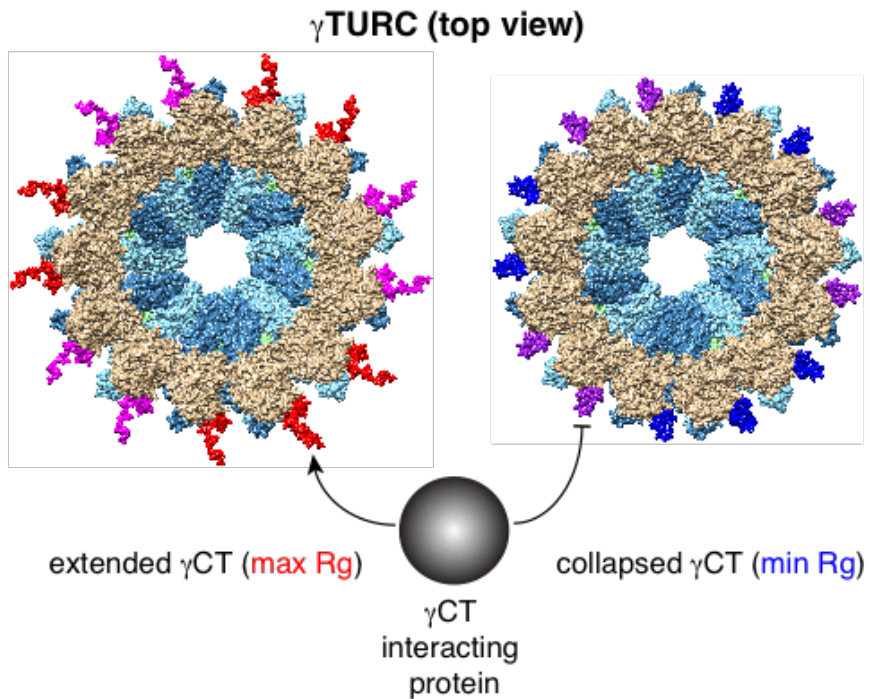


Figure 3–13: γ -TuRC

to a misregulation of the recruitment of microtubule associated proteins and thus a defect in microtubule dynamics. The identity of the protein(s) being recruited by the γ -CT remains an open question but there are several candidates known to affect microtubule stability and localize to the spindle poles are currently being verified through various experimental screens. However, the characterization of γ -CT conformational sampling is an essential first step and a useful tool in identifying these potential interactors and understanding the complex mechanisms by which IDRs regulate large molecular machines.

which candidates

CHAPTER 4

Conclusions

A totally blind process can by definition lead to anything; it can even lead to vision itself.

Jacques Monod

4.0.1 Summary of Findings

In this thesis I presented computational models that shed light on a previously unreported type of IDP dynamics. The collective motion between extended and collapsed states we observed in the phosphorylated γ -CT constitute evidence for an organized disordered ensemble where shifting the equilibrium between sub-regions can give rise to switch-like behaviour without transitions to folded states. Furthermore, we present a detailed physical mechanism to explain the open question of the role of phospho-regulation of the mitotic spindle.

4.0.2 Future Aims

Due to the extremely high computational costs associated with long timescale MD simulations, we are still continuing work on achieving a more complete sampling of the γ -CT conformational space. To this end, we are running replicate simulations to further confirm our findings. However, with the experimental findings from NMR to guide simulations, we are confident that the MD results are sound.

Next, we would like to exploit the remarkably close agreement between NMR and MD to establish a pipeline for further characterizing the physical mechanisms at play in this system. That is, we would like to harness MDS to inform further NMR experiments by making predictions *in silico* of mutants to the γ -CT that would affect the physical mechanism described here in some desired manner. We would then use these predictions to motivate NMR studies which can then go to further validate the mechanism and serve as experimental tools for probing the mechanism *in vivo*. Apart from allowing us to further our understanding of the physical mechanisms of IDRs, functional mutants can serve as a tool for identifying unknown interacting proteins and intra-molecular interactions. We propose to build a high throughput tool for searching the mutational space of IDPs and evaluating dynamic behaviour using a combination of genetic algorithms and MD. Due to the large number of computations this requires, we will have to employ ‘enhanced’ MD sampling techniques such as implicit solvation and replica exchange MD to increase sampling rates. This software is already under development and will serve as a testable hypothesis generation tool that can be applied to understanding the structural mechanisms of any intrinsically disordered system.

CHAPTER 5

Appendix

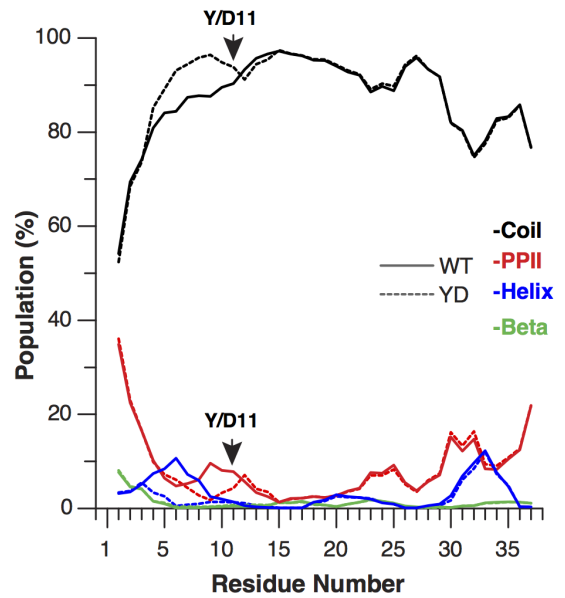


Figure 5–1: NMR Secondary Structure Assignments
Text

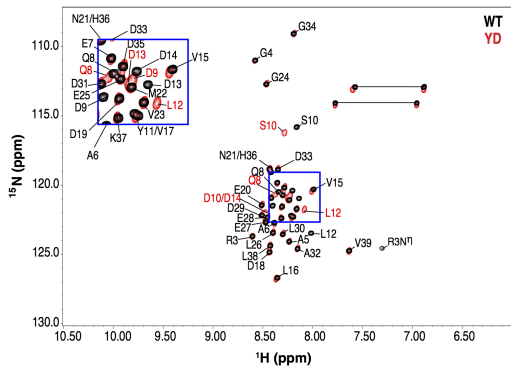


Figure 5–2: NMR Chemical Shifts
Text

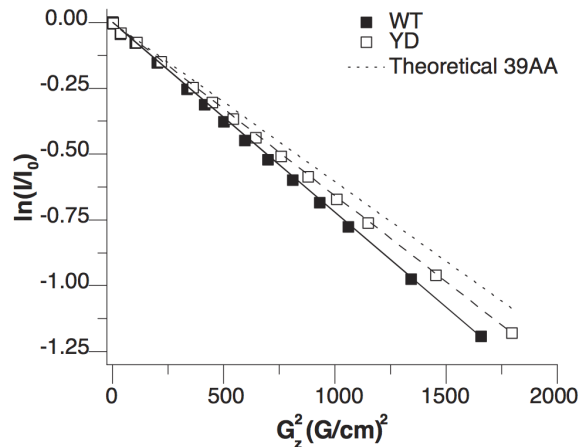


Figure 5–3: NMR Diffusion Measurements
Text

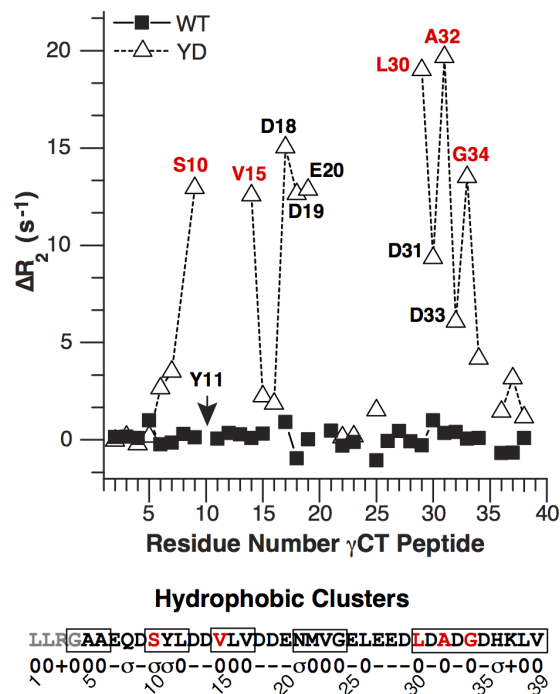
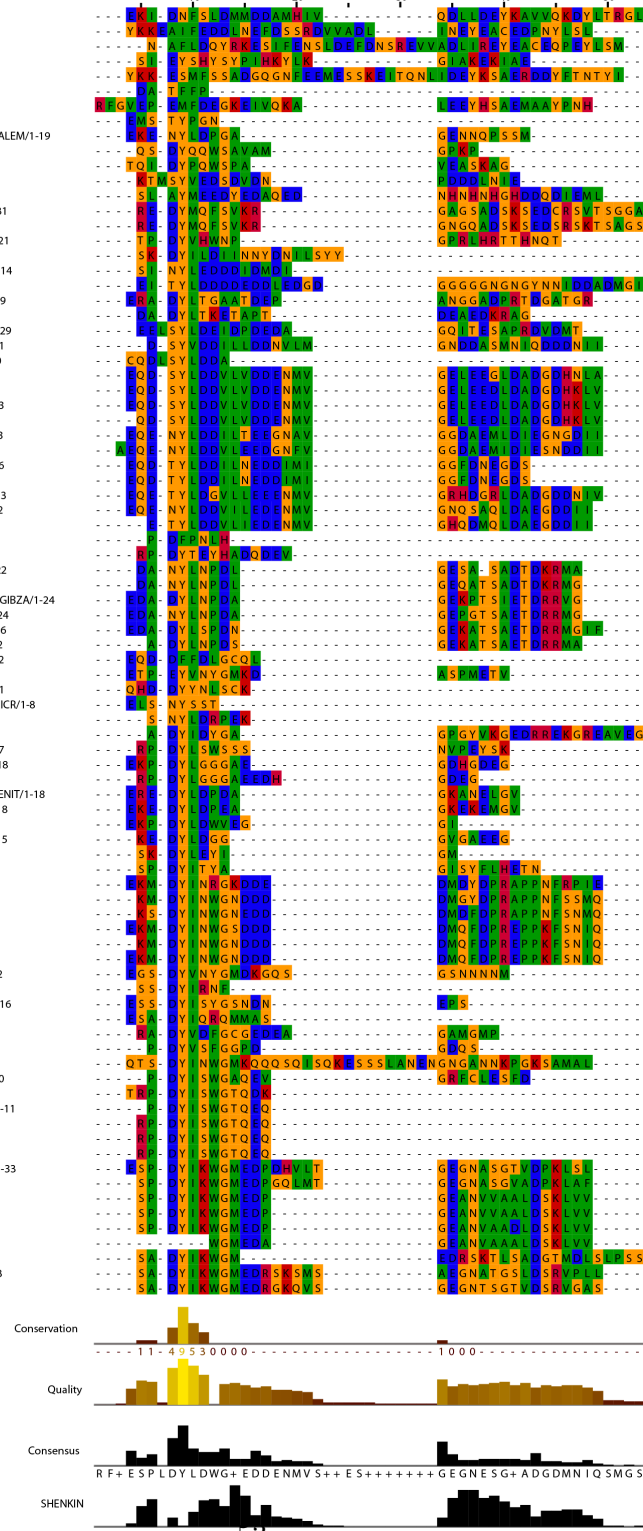


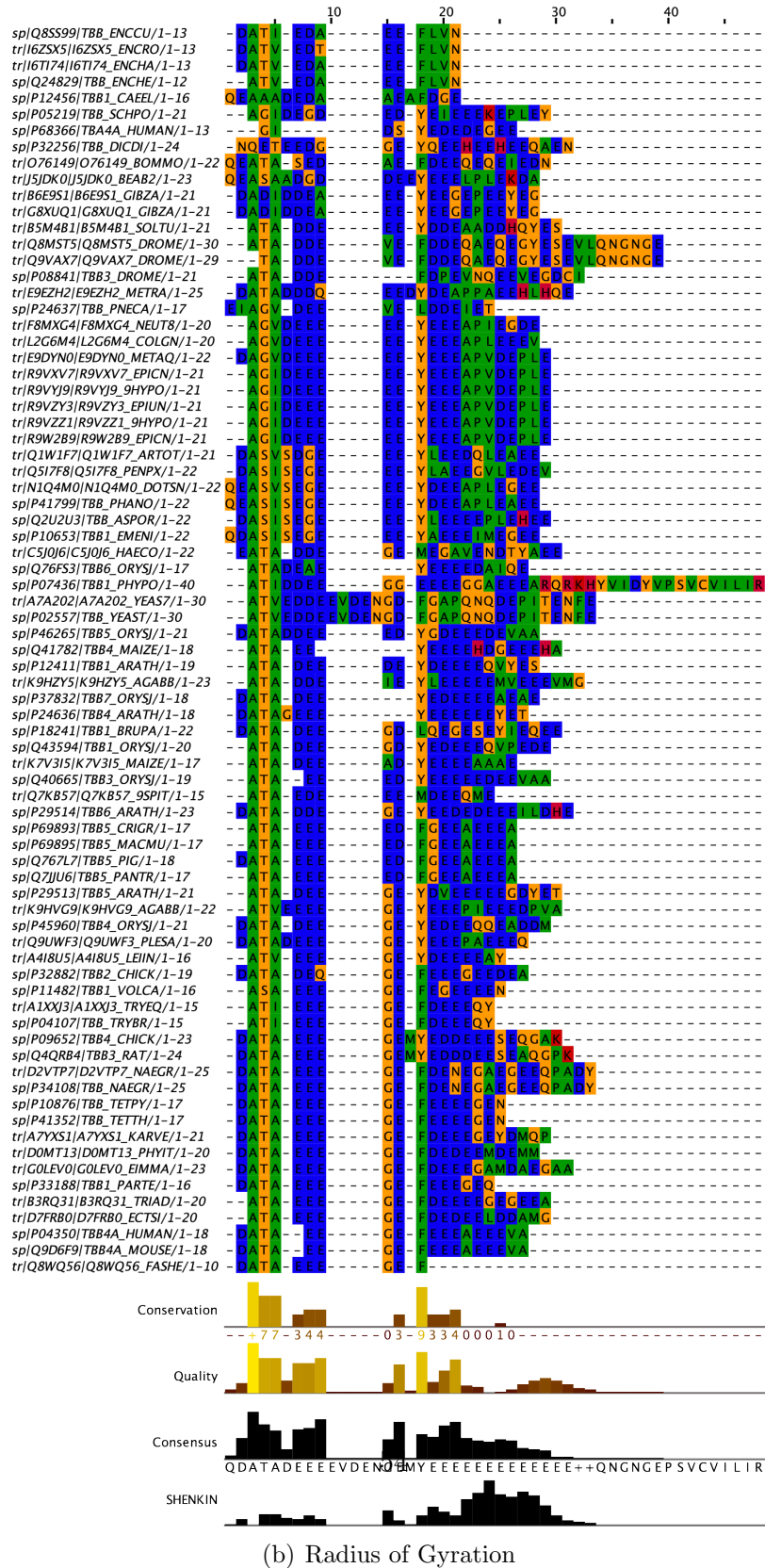
Figure 5–4: NMR Dispersion Measurements
Text

sp|P34475|TBG_CAEEL/1-38
sp|P25295|TBG_SCOPH/1-39
sp|Q9Y882|TBG_SCUPH/1-45
sp|M54041|TBG_ENTHI/1-25
sp|P34787|TBG_PLAFO/1-47
sp|H2F242|H2F242_9CRYP/1-6
sp|Q8S8R2|TBG_ENCUL/1-34
tr|TASR01|TASR01_ENCRL/1-8
tr|B4P141|B4P141_DROGR/1-16
sp|P42271|TBG_BDOME/1-18
sp|C46Z62|C46Z62_PICGP/1-21
tr|B2N5K6B2N5K6_SSORJ/1-31
tr|B3NAN3B1AN3NAN3B_DROER/1-31
tr|B4T21Z|B4T21Z_DROSE/1-31
tr|H9D7W|H9D7W_BOMMO/1-21
sp|Q9SE4A|TBGN_GUITH/1-19
tr|HW8ZB8|HW8ZB8_CAN09/1-14
sp|Q93807|TBG_CANAX/1-37
tr|N1Q9N1|N1Q9N1_PSEFD/1-29
sp|P40633|TBG_COHCZ/1-21
tr|W1QLO8|W1QLO8_OGAPD/1-29
tr|B2N5K8B2N5K8_KLUMA/1-31
tr|B2N6K1|B2N6K1_PICGM/1-20
tr|JB0523|JB0523_SACAR/1-33
tr|C7G1U1|C7G1U1 YEAS2/1-33
tr|C8ZDH6|C8ZDH6 YEAS8/1-33
sp|P53377|TBG_BEAST/1-32
tr|G8WZB5|G8WZB5_EREYC/1-33
sp|T055A4|TBG_ASHGO/1-34
tr|B2N5K7|B2N5K7_CANGB/1-26
sp|O6PNFU9|TBG_CANGA/1-26
tr|G8ZRHO|G8ZRHO_TORDC/1-33
tr|C9V989|C9V989_ZYGRC/1-32
tr|S56E6LG|S56E6LG_ZYG82/1-30
tr|FL14ZB|FL14ZB_A5CSU/1-7
tr|N9RBT0|N9RBT0_WAL9/1-14
tr|F7W64F|F7W64_SORMK/1-22
tr|G2QUB9|G2QUB9_THITE/1-23
tr|A01061PMX3|A01061PMX3_GIBZA/1-24
tr|T7J0M1|T7J0M1_MAGOP/1-24
tr|EP94D2|EP94D2_META0/1-26
tr|AF0KMF1|AF0KMF1_TRIHA/1-21
tr|A7RB2B|A7RB2B_BABBO/1-12
tr|CD59|CD59_BDH9/09-19
tr|Q4N0B6|Q4N0B6_THEPA/1-11
tr|A0A0B2U1|A0A0B2U1_9MCIR/1-8
tr|R4XPB4|R4XPB4_TADPE/1-9
sp|P32348|TBG_UTSP/1-28
tr|MT2Y3ES|MT2Y3ES_GALSU/1-17
tr|C5CFW99|C5CFW99_ARTOC/1-18
tr|P2X2J2|P2X2J2_TRIC/1-7
tr|A0A02LF1|A0A02LF1_PENIT/1-18
tr|G7XNK7|G7XNK7_ASPPK/1-18
tr|V6L6V7|V6L6V7_9EUKA/1-13
tr|C5PW60|C5PW60_COPCP/1-15
tr|E1XEM1|E1XEM1_GIAIA/1-10
tr|F8PS16|F8PS16_BEPUR/9-18
sp|P54404|TBG_EUPCR/1-29
sp|P54404|TBG_EUPCR/1-28
tr|P90548|TBG_EUPCO/1-29
sp|P34786|TBG_EUPOC/1-28
sp|P54402|TBG_EUPOE/1-29
tr|000896|000896_PHYPO/1-22
tr|P09471|P09471_STRYP/1-8
tr|2WLO9W|2WLO9W_MONRO/1-16
tr|Q39582|TBG_CHDLE/1-13
tr|B5Y551|B5Y551_PHATC/1-20
tr|Q72922|TBG_COPCT/1-14
sp|P54045|TBG_BTRF/1-44
tr|C3H2D8|C3H2D8_BRAFL/1-20
sp|P23330|TBG_XENLA/1-13
tr|G3WMD2|G3WMD2_SARHA/1-11
tr|L5JU5L|L5JU5L_RUTE/1-12
sp|P23528|TBG1_HUMAN/1-12
tr|P83887|TBG1_MOUSE/1-12
tr|Q1HM07|Q1HM07_TOBAC/1-33
tr|P38557|TBG2_ARATH/1-32
sp|Q41807|TBG1_MAIZE/1-27
sp|Q41874|TBG2_MAIZE/1-27
sp|Q41808|TBG2_MAIZE/1-27
sp|Q49068|TBG2_ORYSJ/1-21
sp|P34785|TBG_ANEPH/1-29
tr|Q8L81K|Q8L81K_MARAC/1-33
tr|Q9XF3|Q9XF3_TBPH_PAPVA/1-33



55

(a) Representative Structures



(b) Radius of Gyration

Figure 5–4: Tubulin CT Multiple Sequence Alignments
This is the text

References

- [1] Hector Aldaz, Luke M Rice, Tim Stearns, and David A Agard. Insights into microtubule nucleation from the crystal structure of human γ -tubulin. *Nature*, 435(7041):523–527, 2005.
- [2] Rolf Apweiler, Amos Bairoch, Cathy H Wu, Winona C Barker, Brigitte Boeckmann, Serenella Ferro, Elisabeth Gasteiger, Hongzhan Huang, Rodrigo Lopez, Michele Magrane, et al. Uniprot: the universal protein knowledgebase. *Nucleic acids research*, 32(suppl 1):D115–D119, 2004.
- [3] Roby P Bhattacharyya, Attila Reményi, Matthew C Good, Caleb J Bashor, Arnold M Falick, and Wendell A Lim. The ste5 scaffold allosterically modulates signaling output of the yeast mating pathway. *Science*, 311(5762):822–826, 2006.
- [4] Norman E Davey, Gilles Travé, and Toby J Gibson. How viruses hijack cell regulation. *Trends in biochemical sciences*, 36(3):159–169, 2011.
- [5] J Garcia De la Torre, ML Huertas, and B Carrasco. Hydronmr: prediction of nmr relaxation of globular proteins from atomic-level structures and hydrodynamic calculations. *Journal of Magnetic Resonance*, 147(1):138–146, 2000.
- [6] Marileen Dogterom, Jacob WJ Kerssemakers, Guillaume Romet-Lemonne, and Marcel E Janson. Force generation by dynamic microtubules. *Current opinion in cell biology*, 17(1):67–74, 2005.
- [7] Robert C Edgar. Muscle: multiple sequence alignment with high accuracy and high throughput. *Nucleic acids research*, 32(5):1792–1797, 2004.
- [8] Marcos RM Fontes, Trazel Teh, and Bostjan Kobe. Structural basis of recognition of monopartite and bipartite nuclear localization sequences by mammalian importin- α . *Journal of molecular biology*, 297(5):1183–1194, 2000.

- [9] Stefano Gianni, Angela Morrone, Rajanish Giri, and Maurizio Brunori. A folding-after-binding mechanism describes the recognition between the trans-activation domain of c-myb and the kix domain of the creb-binding protein. *Biochemical and biophysical research communications*, 428(2):205–209, 2012.
- [10] Thomas A Graham, Denise M Ferkey, Feng Mao, David Kimelman, and Wenzing Xu. Tcf4 can specifically recognize β -catenin using alternative conformations. *Nature Structural & Molecular Biology*, 8(12):1048–1052, 2001.
- [11] William Humphrey, Andrew Dalke, and Klaus Schulten. Vmd: visual molecular dynamics. *Journal of molecular graphics*, 14(1):33–38, 1996.
- [12] Harish C Joshi, Monica J Palacios, Leemore McNamara, and Don W Cleveland. γ -tubulin is a centrosomal protein required for cell cycle-dependent microtubule nucleation. 1992.
- [13] Wolfgang Kabsch and Christian Sander. Dictionary of protein secondary structure: pattern recognition of hydrogen-bonded and geometrical features. *Biopolymers*, 22(12):2577–2637, 1983.
- [14] E Karsenti and I Vernos. The mitotic spindle: a self-made machine. *Science*, 294(5542):543–547, 2001.
- [15] Jamie M Keck, Michele H Jones, Catherine CL Wong, Jonathan Binkley, Daici Chen, Sue L Jaspersen, Eric P Holinger, Tao Xu, Mario Niepel, Michael P Rout, et al. A cell cycle phosphoproteome of the yeast centrosome. *Science*, 332(6037):1557–1561, 2011.
- [16] Justin M Kollman, Charles H Greenberg, Sam Li, Michelle Moritz, Alex Zelter, Kimberly K Fong, Jose-Jesus Fernandez, Andrej Sali, John Kilmartin, Trisha N Davis, et al. Ring closure activates yeast γ turc for species-specific microtubule nucleation. *Nature structural & molecular biology*, 22(2):132–137, 2015.
- [17] Justin M Kollman, Andreas Merdes, Lionel Mourey, and David A Agard. Microtubule nucleation by γ -tubulin complexes. *Nature reviews Molecular cell biology*, 12(11):709–721, 2011.
- [18] Donna F Kubai. The evolution of the mitotic spindle. *International review of cytology*, 43:167–227, 1976.

- [19] Albert H Mao, Scott L Crick, Andreas Vitalis, Caitlin L Chicoine, and Rohit V Pappu. Net charge per residue modulates conformational ensembles of intrinsically disordered proteins. *Proceedings of the National Academy of Sciences*, 107(18):8183–8188, 2010.
- [20] William E Meador, Anthony R Means, and Florante A Quiocho. Target enzyme recognition by calmodulin: 2.4 a structure of a calmodulin-peptide complex. *Science*, 257(5074):1251–1255, 1992.
- [21] Tanja Mittag and Julie D Forman-Kay. Atomic-level characterization of disordered protein ensembles. *Current opinion in structural biology*, 17(1):3–14, 2007.
- [22] Ishwar Radhakrishnan, Gabriela C Pérez-Alvarado, David Parker, H Jane Dyson, Marc R Montminy, and Peter E Wright. Solution structure of the kix domain of cbp bound to the transactivation domain of creb: a model for activator: coactivator interactions. *Cell*, 91(6):741–752, 1997.
- [23] Peter Tompa. Intrinsically disordered proteins: a 10-year recap. *Trends in biochemical sciences*, 37(12):509–516, 2012.
- [24] Peter Tompa and Monika Fuxreiter. Fuzzy complexes: polymorphism and structural disorder in protein–protein interactions. *Trends in biochemical sciences*, 33(1):2–8, 2008.
- [25] Jacalyn Vogel, Ben Drapkin, Jamina Oomen, Dale Beach, Kerry Bloom, and Michael Snyder. Phosphorylation of γ -tubulin regulates microtubule organization in budding yeast. *Developmental cell*, 1(5):621–631, 2001.
- [26] Jacalyn Vogel and Michael Snyder. The carboxy terminus of tub4p is required for gamma-tubulin function in budding yeast. *Journal of cell Science*, 113(21):3871–3882, 2000.
- [27] Deborah K Wilkins, Shaun B Grimshaw, Véronique Receveur, Christopher M Dobson, Jonathan A Jones, and Lorna J Smith. Hydrodynamic radii of native and denatured proteins measured by pulse field gradient nmr techniques. *Biochemistry*, 38(50):16424–16431, 1999.
- [28] Peter E Wright and H Jane Dyson. Linking folding and binding. *Current opinion in structural biology*, 19(1):31–38, 2009.

- [29] Peter E Wright and H Jane Dyson. Intrinsically disordered proteins in cellular signalling and regulation. *Nature Reviews Molecular Cell Biology*, 16(1):18–29, 2015.
- [30] Hongtao Yu, James K Chen, Sibo Feng, David C Dalgarno, Andrew W Brauer, and Stuart L Schreiber. Structural basis for the binding of proline-rich peptides to sh3 domains. *Cell*, 76(5):933–945, 1994.
- [31] Tsaffrir Zor, Bernhard M Mayr, H Jane Dyson, Marc R Montminy, and Peter E Wright. Roles of phosphorylation and helix propensity in the binding of the kix domain of creb-binding protein by constitutive (c-myb) and inducible (creb) activators. *Journal of Biological Chemistry*, 277(44):42241–42248, 2002.